nagra.

Arbeitsbericht NAB 13-56

Thermo-hydraulic modelling of the temperature distribution in the siting region Nördlich Lägern

July 2014

A. Papafotiou, R. Senger
Intera

**Nationale Genossenschaft
für die Lagerung
radioaktiver Abfälle**

Hardstrasse 73
CH-5430 Wettingen
Telefon 056-437 11 11

www.nagra.ch

nagra.

Arbeitsbericht NAB 13-56

Thermo-hydraulic modelling of the temperature distribution in the siting region Nördlich Lägern

July 2014

A. Papafotiou, R. Senger
Intera

KEYWORDS
Thermo-hydraulic modelling, Nördlich Lägern, temperature distribution, groundwater

Nationale Genossenschaft für die Lagerung radioaktiver Abfälle

Hardstrasse 73
CH-5430 Wettingen
Telefon 056-437 11 11

www.nagra.ch

Nagra Working Reports concern work in progress that may have had limited review. They are intended to provide rapid dissemination of information. The viewpoints presented and conclusions reached are those of the author(s) and do not necessarily represent those of Nagra.

Zusammenfassung

Für die Einengung der möglichen Standortgebiete im Rahmen der Etappe 2 des Sachplans geologische Tiefenlager auf mindestens 2 Standortgebiete je Abfallart müssen alle Gebiete im Rahmen des sicherheitstechnischen Vergleichs umfassend bewertet werden. In diese Bewertung fliessen neben zahlreichen anderen Aspekten auch die thermo-hydraulischen Zustände der jeweiligen Standortgebiete mit ein. Der vorliegende Bericht beschreibt die zu diesem Zweck durchgeführten thermo-hydraulischen Simulationen für das Standortgebiet Nördlich Lägern.

Die hydraulischen Simulationen, die die Grundlage für die hier vorgestellten thermo-hydraulischen Simulationen bilden, sind umfassend in Luo et al. (2014) beschrieben. Die zusätzlich benötigten Parameter und Randbedingungen, die für die vorliegenden Simulationen genutzt wurden, beruhen hauptsächlich auf geophysikalischen Messungen der Tiefbohrung Weiach bzw. der nahegelegenen Tiefbohrung Benken, aus denen durch 1D Inversionen die benötigten Parameter errechnet wurden.

Es wurden insgesamt 5 Fälle berechnet, die sich durch unterschiedliche Annahmen bezüglich der thermischen Randbedingungen unterscheiden. Der Referenzfall bezieht sich auf ein steady-state Szenario, bei dem die Randbedingungen aus den 1D Inversionen der Messwerte aus den Tiefbohrungen entnommen wurden. Die Ergebnisse zeigen die zu erwartende Zunahme der Temperatur mit zunehmender Tiefe, die maximalen Temperaturen werden im tiefsten Teil des Modells erreicht.

Während den regionalen Störungen im Referenzfall eine Durchlässigkeit von 1e-7 m/s zugewiesen wurde, werden diese Flächen in Variante 1 mit Durchlässigkeiten von 1e-15 m/s belegt. Dies ermöglicht es, die Rolle von Störungen, die bei geeigneten Durchlässigkeiten einen Austausch von Grundwasser auch zwischen den hydrogeologischen Einheiten erlauben, abzuschätzen. Die Ergebnisse dieser Simulation zeigen, dass im Allgemeinen die Temperaturen etwas höher sind als im Referenzfall, da kein Grundwasseraustausch zwischen den einzelnen hydrogeologischen Einheiten entlang der Störungen möglich ist.

Variante 2 unterscheidet sich vom Referenzfall durch die Annahme von abnehmenden Temperaturen an der Oberfläche, so dass, wenn auch vereinfacht, der Einfluss von Eiszeiten abgeschätzt werden kann. Es zeigt sich, dass bei gleichbleibendem basalen Wärmefluss und abnehmenden Oberflächentemperaturen auch im Untergrund tiefere Temperaturen gemessen werden. Diese treten zeitlich versetzt ein, da die Änderungen der Oberflächentemperatur nur langsam bis in tiefere Bereiche des Modells propagieren.

Während in den zuvor beschriebenen Varianten sowie im Referenzfall ein einheitlicher basaler Wärmefluss angewandt wurde, wurde dieser für Variante 3 räumlich variiert. Es wurde ein von Ost nach West linear zunehmender, basaler Wärmefluss zugewiesen, um so die Temperaturanomalien im Raum Bad Zurzach - Unteres Aaretal (westlich des Modelliergebiets) zu berücksichtigen. Die aus dieser Variante resultierenden Temperaturen zeigen im Vergleich zum Referenzfall niedrigere Temperaturen im Osten (hier ist, wieder im Vergleich zum Referenzfall, der basale Wärmefluss niedriger) und höhere Temperaturen im Westen (hier ist der basale Wärmefluss höher als im Referenzfall). Ausserdem zeigen die Simulationen, dass untiefe Bereiche deutlich von den Oberflächentemperaturen beeinflusst werden, während in tieferen Bereichen der basale Wärmefluss die Temperaturverteilung dominiert.

Variante 4 unterscheidet sich vom Referenzfall durch eine zusätzlich radiogene Wärmeproduktion der im Modell berücksichtigten Einheiten; im Referenzfall wurde diese zusätzliche Wärmequelle vernachlässigt. Diese zusätzliche Wärme entsteht beim Zerfall radioaktiver Isotope bestimmter Minerale. Die Ergebnisse der Simulationen dieser Variante zeigen jedoch praktisch keine Auswirkung auf die Temperaturverteilung im Untergrund. Dies zeigt, dass der basale Wärmefluss bzw. die Oberflächentemperatur einen weitaus höheren Einfluss auf die erreichten Temperaturen hat als die radiogene Wärmeproduktion der berücksichtigten Einheiten im Modell.

Zusammenfassend kann festgehalten werden, dass wie erwartet die Temperaturen im Untergrund massgeblich vom basalen Wärmefluss, den hydraulischen Eigenschaften der Störungen und der Oberflächentemperatur beeinflusst werden. Andere Effekte wie die hydrogeologischen Verhältnisse abseits von Störungen oder die radiogene Wärmeproduktion der Gesteine selber haben keine bzw. nur vernachlässigbar kleine Auswirkung auf die Temperaturverteilung im Untergrund des Modellgebiets Nördlich Lägern.

Table of Contents

List of Tables

List of Figures

1 Introduction

1.1 Background

The road map and criteria for the selection of repository sites for radioactive waste in Switzerland are defined with the Sectoral Plan for Deep Geological Repositories / AGT (SFOE 2008). Based on this plan, the site selection process for the realization of SF/HLW and L/ILW deep geological repositories comprises three stages. Based on safety and technical feasibility criteria, SGT / Stage 1 led to the proposal of six geologically suitable siting regions for the L/ILW repository (Südranden, Zürich Nordost, Nördlich Lägern, Jura Ost, Jura-Südfuss and Wellenberg) and three regions for the SF/HLW repository (Zürich Nordost, Nördlich Lägern, Jura Ost) as illustrated in Figure 1-1. SGT / Stage 2 requires the selection of at least two sites for L/ILW and SF/HLW repositories based on provisional safety analyses and engineering feasibility studies performed for all repository configurations in the selected sites. Among other things, the provisional safety analyses and the engineering feasibility studies require a set of thermal (boundary) conditions at, or in the vicinity of, the repository. In this context, coupled numerical models of groundwater and heat flow are developed on different scales of interest comprising the repository near-field, the local scale relevant to the siting region, and the regional scale describing the regional hydrologic conditions in northern Switzerland. The numerical analyses of groundwater flow on these scales are discussed separately in Gmünder et al. (2013) and Luo et al. (2013). This report documents a supplementary analysis of the subsurface thermal effects coupled with groundwater flow. For this, a comprehensive database of geothermal data is compiled and implemented in a numerical model developed on the local scale for the siting region Nördlich Lägern.

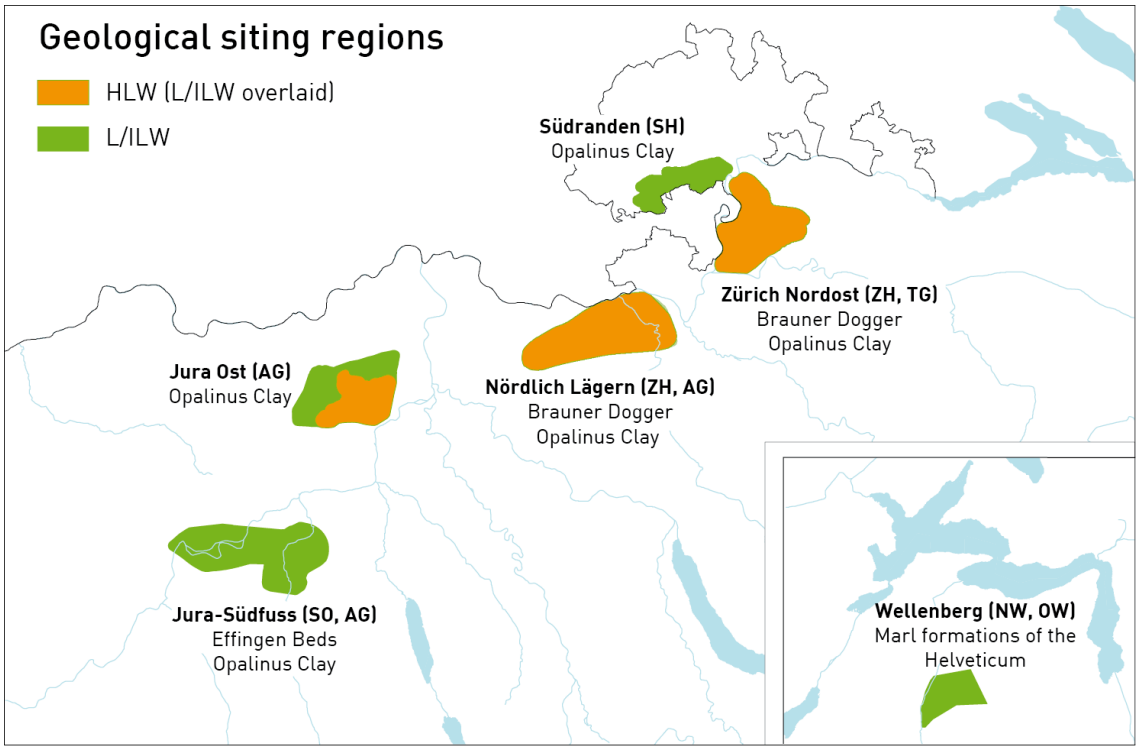

Fig. 1-1: Potential siting regions and host rocks for geological disposal of low- and intermediate-level (L/ILW) and high-level (HLW) radioactive waste in Switzerland (after Nagra 2008).

1.2 Objectives

Analysis of the coupled thermal-hydraulic evolution of the potential siting regions includes several steps ranging from the compilation of available geothermal information to model calibrations, comparisons between different model approaches and finally simulation of different scenarios that are required by the provisional safety analyses. The objectives of this work scope are the following:

- Survey of available field, laboratory and model data and compilation of a database of geothermal properties that will be available for implementation in the current model as well as in further thermal-hydraulic modelling.
- A workflow for additional thermal-hydraulic modelling studies (i.e. for other siting regions).
- Estimation of ambient host-rock temperatures under consideration of the site-specific combined hydrogeological and geothermal conditions.
- Evaluation of the impact of hydraulic conditions and ambient groundwater gradients prevailing in the siting regions on heat flow.
- Evaluation of heat flow associated with subsurface structures (i.e. fault zones) and the relevant impact on hydraulic conditions and groundwater gradients.
- Evaluation of the impact of ice ages on the thermal-hydraulic evolution of the siting regions and the associated temperatures and hydraulic gradients prevailing in the repository near-field.

- Uncertainty assessment introduced by geothermal properties with limited amount of available data, such as radiogenic heat emission and spatial variability of basal heat flow.
- Supply of input and boundary conditions for site-specific safety analyses with special focus on the assessment of repository induced effects (heat, gas, chemical interaction etc.)

2 Hydrogeological and geothermal setting

The development of numerical models that can adequately describe the thermo-hydraulic evolution in Nördlich Lägern requires extensive knowledge on the prevailing hydrogeological and thermal conditions of the area. This background will be provided in this chapter. Section 2.1 provides an overview of the geological background in Northern Switzerland associated with the investigated area. A closer look at the hydrogeological setting in Nördlich Lägern, comprising information on the main aquifers, aquitards and water-conducting features, is given in Section 2.2. Finally, available knowledge and field databases relevant to the geothermal conditions and thermal rock properties in the region are compiled and discussed in Section 2.3.

2.1 Geological background

As indicated in Figure 2-1, the siting regions selected in the SGT / Stage 1, except Wellenberg, are located within northern Switzerland. For the SF/HLW the potential host-rock is the Opalinus Clay, the hostrocks for the L/ILW are the Opalinus Clay, the 'Brown Dogger', the Effinger Member and the Helvetic Marl. Except the latter, these are sedimentary formations that belong to the Mesozoic sedimentary sequence of northern Switzerland, dipping gently to the south/southeast. The sedimentary sequence in the region is presumably autochthone in the Tabular Jura towards the north and near the Rhine river. South- and westwards from the Jura Main Thrust and along the Folded Jura, the sedimentary rocks are sheared off and folded through a series of thrust-related faults. The Folded Tabular Jura in the north is less intensively deformed. Further south and across the Folded Jura in north-central Switzerland these are overlain by Tertiary Molasse and Quaternary sediments. The sedimentary sequences are deposited on a crystalline basement, interrupted by Permocarboniferous troughs that mainly run from west/southwest to east/northeast. Currently, the most significant known structure is the Weiach trough delineated in the south by the Baden-Irchel-Herdern Lineament and in the north by a series of thrusts and flexures along the Swiss-German border.

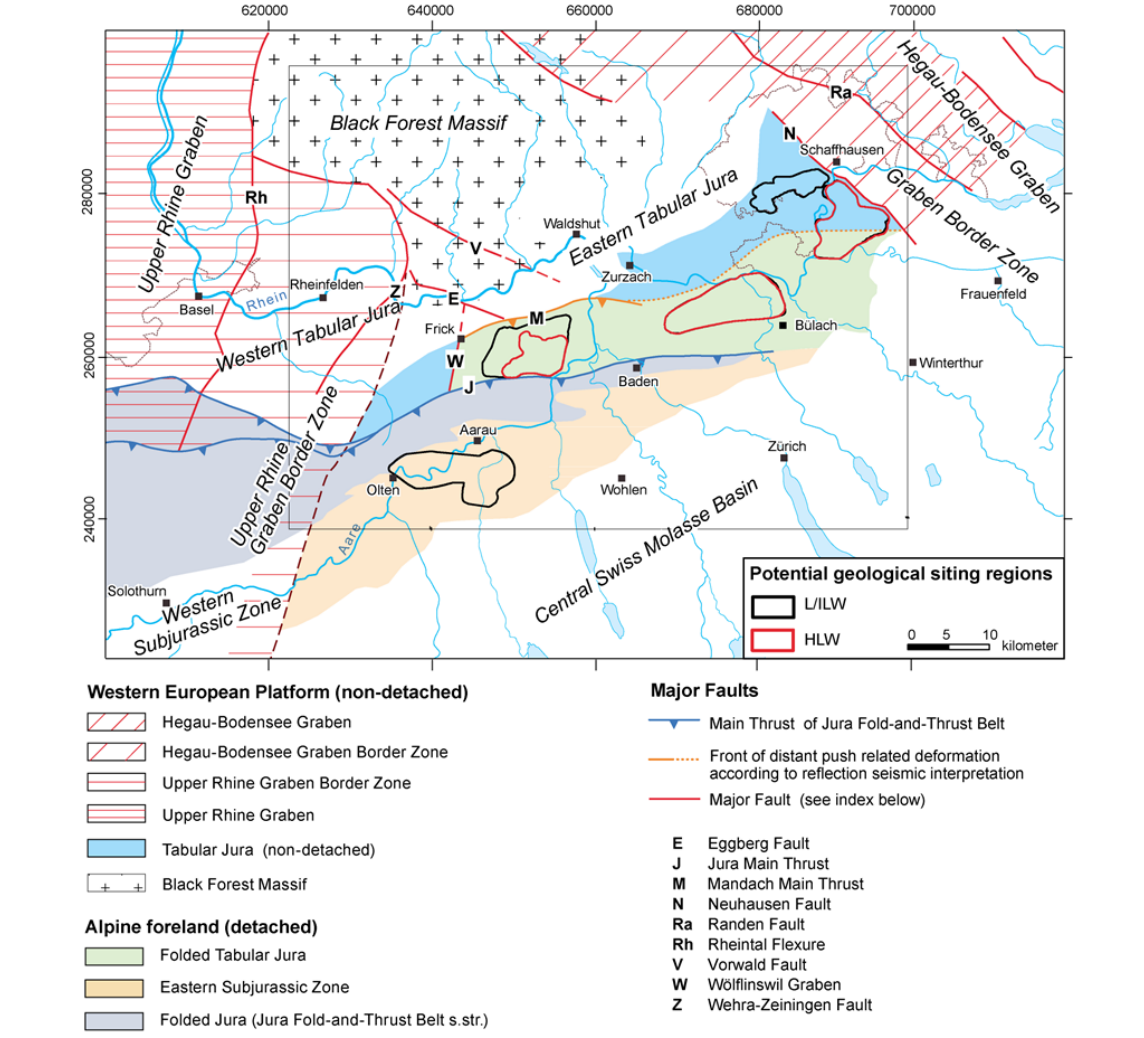

West-East

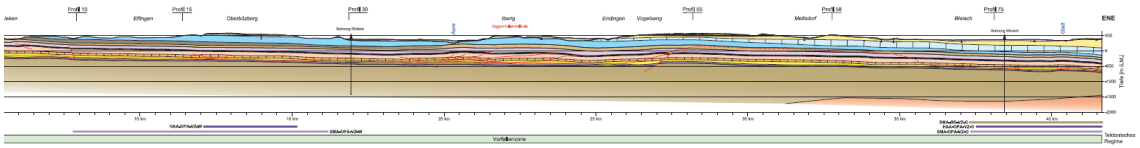

North/NorthWest - South/SouthEast

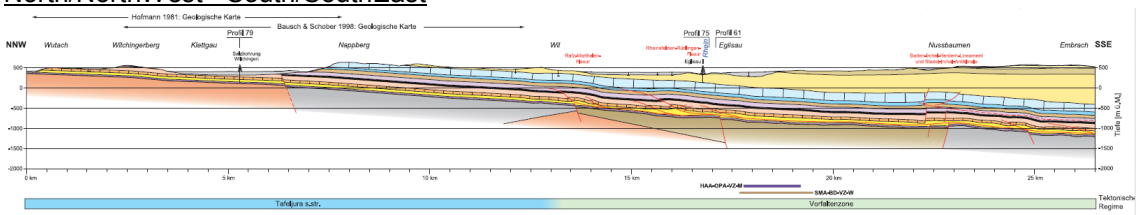

Fig. 2-1: Approximation of tectonic regimes in northern Switzerland (top) and corresponding stratigraphic cross-sections in the west-east and north/northwest-south/southeast direction (bottom). (modified from Nagra 2008)

2.2 Hydrogeological setting Nördlich Lägern

Due to the different lithology of the individual layers found in the Mesozoic sedimentary rocks, the sedimentary stack can roughly be regarded as a sequence of alternating aquifers and aquitards. Combined with the hydrologic conditions in the region, these determine the hydrogeology of each of the siting regions. For Nördlich Lägern, the lithostratigraphic profile adopted for the hydrogeological analyses is mainly based on the Weiach borehole (see Fig. 2-2).

The main lithostratigraphic units distinguished here and also in the hydrogeological model are shortly described below. Note that the regional and local stratigraphy has recently been revised (see e.g. Bläsi et al. 2013; Deplazes et al. 2013; Bitterli-Dreher 2012 or Reisdorf et al. 2011 for a recent stratigraphy). In this report, the stratigraphy according to the regional geological model of Gmünder et al. (2013a) is used which is mainly based on the stratigraphy as defined in Nagra (2010).

- Muschelkalk: The Muschelkalk is the middle of three lithostratigraphic units within the Trias. In the area of interest, the Muschelkalk is divided into the Upper Muschelkalk (top), the Anhydritgruppe (middle) and the Wellengebirge (lowermost unit of the Muschelkalk, not specifically part of the model domain). The upper Muschelkalk is considered as a regional fractured aquifer, locally appearing also as a karst aquifer. The outcrops of the Muschelkalk are found northwards from the siting region Nördlich Lägern and along the Wutach. Along the Rhine north and northwest from Bad Zurzach, the Muschelkalk comes in direct contact with shallow Quaternary aquifers.
- Keuper: The sediments of the Keuper, the upper lithostratigraphic unit of the Trias, can be separated into the Upper Middlekeuper and Gipskeuper. The Gipskeuper in the model is treated as an aquitard comprised of dolomitic clays, clayey marls, and anhydrite layers with low permeability. The Upper Middlekeuper also contains clay-rich sediments dolomites (Gansinger Dolomite) and some sandstone layers (Stubensandstein and Schilfsandstein Formations), parts of the Upper Middlekeuper are therefore, in the model, treated as a local aquifer with outcrops along the southern bank of the Wutach.
- Lias: The Staffelegg Formation (the stratigraphic unit comprising all Lias sediments) is characterized by heterogenous clay-rich rocks with some limestones and subordinately sandstones. A notable calcareous-rich layer is formed by the Arietenkalk. However, isotopic and hydrochemical evidence show that ground-water flow in these potentially transmissive hydrogeological units is rather small due to limited hydraulic interconnectedness with long potential pathways to the biosphere.
- Opalinus Clay: a potential host-rock for L/ILW and SF/HLW repositories comprising low-permeable claystone that locally becomes silty to sandy. In this typically 80-120 m thick formation, advective groundwater flow is practically absent and transport is dominated by diffusion.
- 'Brown Dogger': The sediments comprising the so called ‘Brown Dogger’ in the area of interest are comprised of a thick succession of clay-rich rocks with local intercalations of siltstones, marls, sandstones, iron oolithes and limestones. It is typically low-permeable with potentially transmissive units (sandy limestones, calcareous-rich iron oolithes) occurring in thin, more permeable horizons especially wihtin the Passwang Formation. Similar to the Lias, these potentially transmissive units lack connectivity. The ‘Brown Dogger’ is also a potential hos-rock for an L/ILW repository.
- Malm: The lithostratigraphic unit of "Malm" in general is divided into Wildegg Formation (including the Effingen Member), Villigen Formation, Schwarzbach Formation and Felsen-kalk Formation. The limestones of the Villigen Formation and the Felsenkalk Formation are

considered to be a regional fracture- and karst- aquifer. Groundwater from this aquifer has a high salinity. The Malm aquifer forms a thin outcrop along the northern boundary of the model domain of Nördlich Lägern.

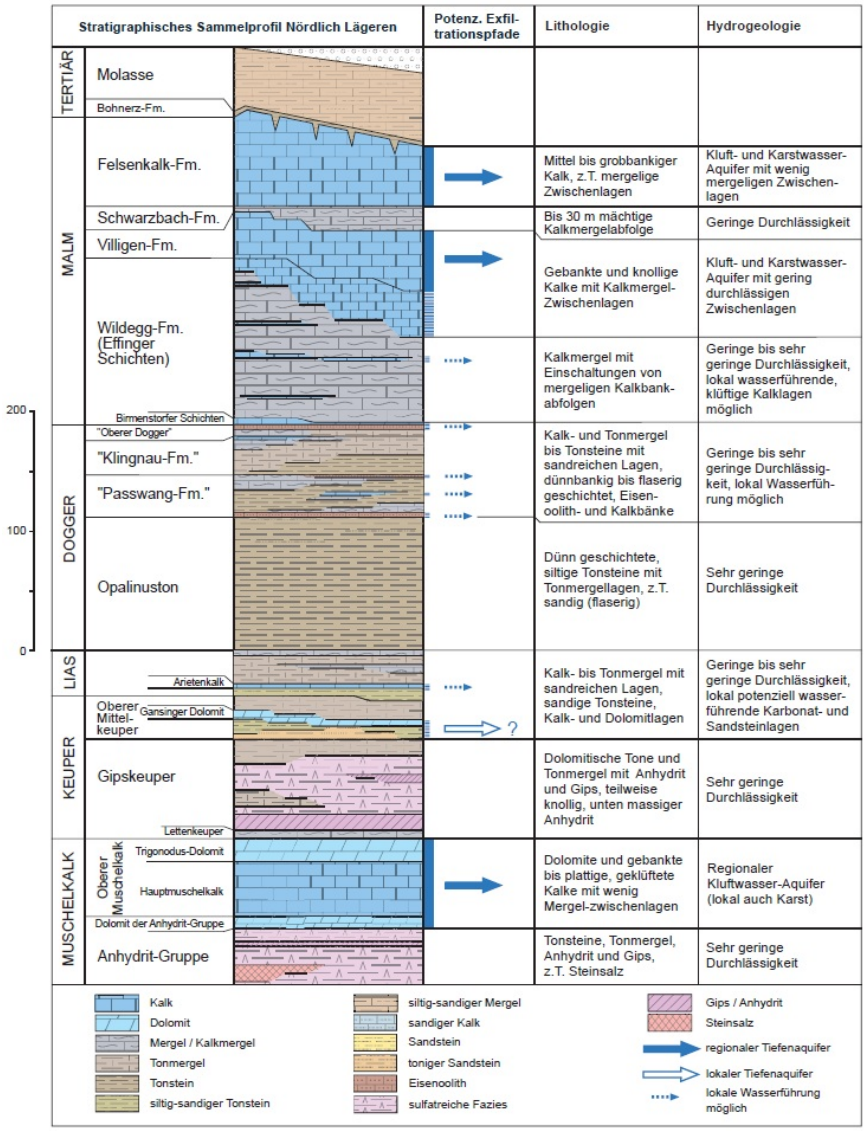

Fig. 2-2: Stratigraphic - hydrogeological profile of the sedimentary rocks in the siting region Nördlich Lägern (Nagra 2010). Major aquifers are indicated with blue thick arrows. Local aquifers are indicated by blue, hollow arrows, potential locally transmissive units confined in low-permeable formations are indicated with blue dashed arrows.

Transport properties in the above mentioned aquifers and/or potentially transmissive units depend strongly on groundwater gradients imposed by regional conditions. In general, hydraulic heads in the Malm aquifer increase along the formation dip from the outcrops in the northwest to the deeper parts of the Malm in southeast. In the Nördlich Lägern region, hydraulic heads additionally show a decrease toward the Rhine indicating a hydraulic connection. A similar behavior is depicted by the hydraulic-head contours of the Muschelkalk Aquifer, showing decreasing heads toward the Rhine and the Aare. A more detailed analysis of regional groundwater gradients on the basis of hydraulic head isolines for the Muschelkalk, Keuper Aquifer and Malm aquifers for the region of Northern Switzerland is provided in Gmünder et al. (2013), with the local situation in Nördlich Lägern described in detail in Luo et al. (2014).

The main fault structures relevant to the local hydrogeological regime in the siting region Nördlich Lägern is the Baden-Irchel-Herdern Lineament spanning in a west-southwest to east-northeast direction along the southern part of the region, and the Ruemi Fault, a fault associated with the Siglistorf Anticline spanning west-northeast. The most dominant hydrologic features are the Rhine crossing the central and northern part of the siting region in west-east direction and the Glatt entering the region from the south to merge with the Rhine.

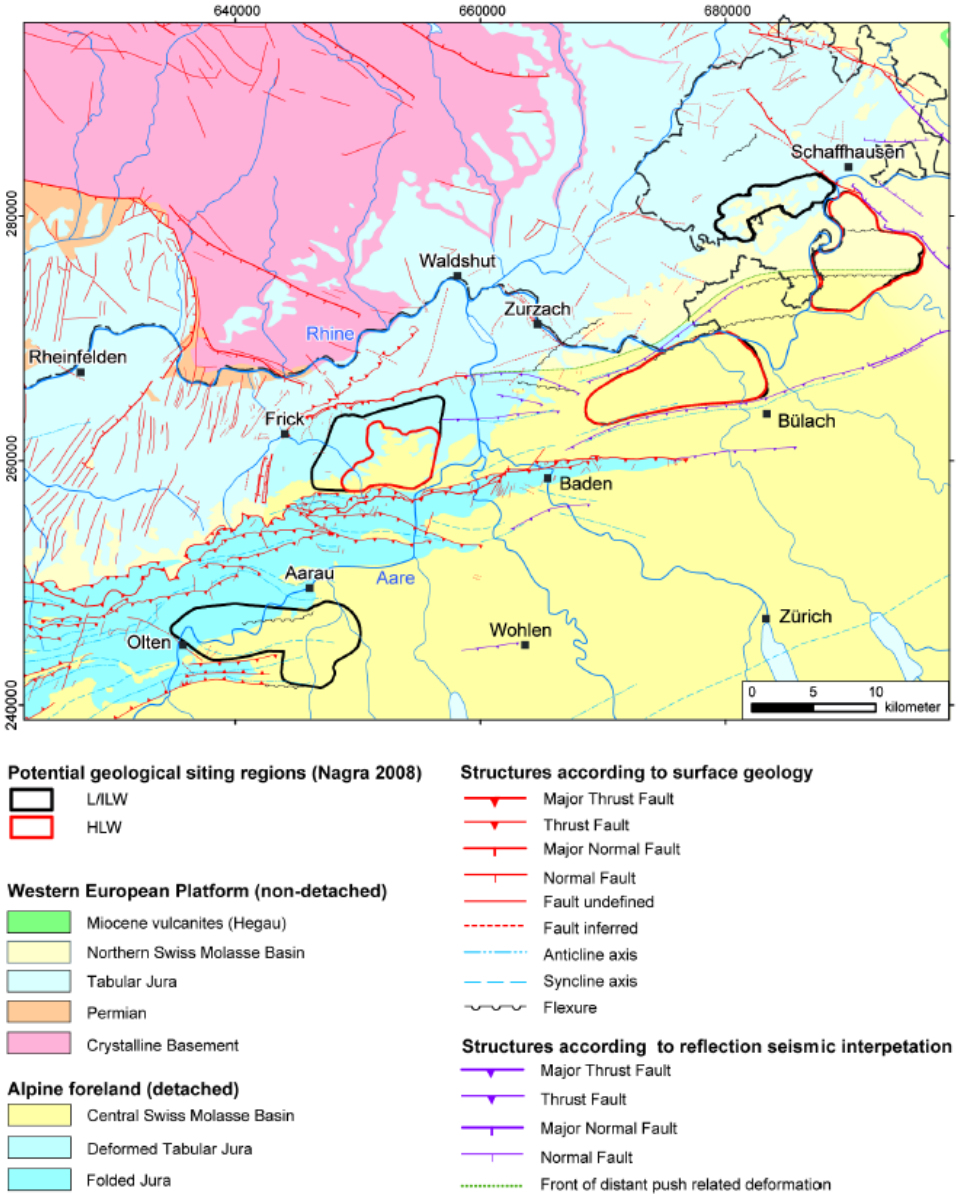

Fig. 2-3: Main tectonic regimes and structures in the siting regions in north-easten Switzerland (Madritsch and Hammer 2012).

2.3 Geothermal setting and thermal rock properties

Predictions of the thermo-hydraulic evolution in the siting region Nördlich Lägern require knowledge of the current geothermal conditions in the area. These are determined by regional heat fluxes and the way heat is conducted and perturbed in the hydrogeological setting. Heat originates from basal heat flow through the base rock, as well as from emissions of radiogenic heat from the rocks themselves. Consequently, heat is transmitted by means of conduction and convection through the saturated geologic formations. The geothermal setting is thus determined on one hand by the ability of the saturated rocks to store and transfer thermal energy and on the other hand by hydraulic gradients associated with groundwater flow that may perturb heat flow patterns. The thermal properties used to describe transfer and storage of heat in rock formations are typically the rock heat conductivity and the specific heat capacity. In the context of modeling heat transport processes, the distribution of these factors determines temperature

gradients and temperature-depth profiles in the subsurface that can be used to calibrate and verify numerical models.

2.3.1 Sources of heat

Basal heat flow typically is the most significant source of heat in a geothermal setting. The amount of heat flux originating from a basal base rock is typically estimated with inverse modeling based on deep borehole measurements of temperature and rock thermal properties. Heat flow calculated using thermal conductivities measured in core samples and measured temperature profiles in the Weiach borehole was found equal to 120 mW/m² (Nagra 1988). Additionally, maps of heat flow at the surface are given in Schill et al (2010).

In addition to the basal heat flow, natural radiogenic heat emission contributes to the amount of heat stored and transferred in the rock formations. Heat produced by the sedimentary formations and crystalline basement found in Nördlich Lägern was determined by Nagra and the Institute of Geophysics of the ETH Zürich based on Gamma-Spectrometer logs in the Weiach and Böttstein boreholes (Schärli and Kohl 2002). The resulting heat production rate values are depicted in Figure 2-4. The average heat production rate for the sedimentary geological formations (Quaternary, Tertiary, Malm, Dogger, Lias, Keuper and Muschelkalk) is equal to 0.5 µW/m³. For the Permocarbon and the crystalline basement, the average heat production rate is 2.5 µW/m³.

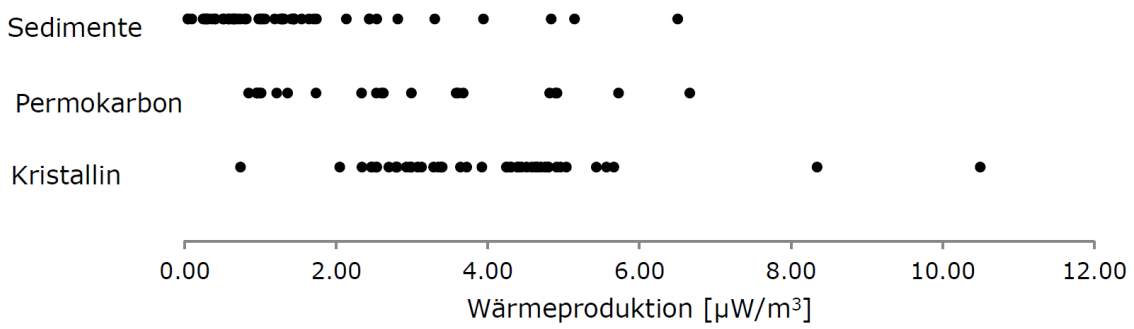

Fig. 2-4: Heat production rates measured in Weiach and Böttstein (from Ollinger and Baujard 2012).

2.3.2 Thermal properties – experimental database

As mentioned in the previous section, the key rock properties in determining heat flow through geologic formations are rock heat conductivity and specific heat capacity.

A dataset of heat conductivities in the geologic formations in Weiach is provided through core sample measurements (Nagra 1988). Vertical profiles of heat conductivities derived from these measurements are shown in Figure 2-5. Based on these values, arithmetic averages per 100 m increments have been derived and compared to the corresponding lithostratigraphic profile from Weiach, as depicted in Figure 2-6. Due to the anhydrite-rich layers, the Keuper formation has the highest thermal conductivities with an average value of 4.0 W/m/K. Similarly, increased thermal conductivities are observed in other formations rich in anhydrite (Muschelkalk) and carbonates (e.g. Malm). Measurements between 554 and 666 m depth indicate an average thermal conductivity value for Opalinus Clay of approximately 2.0 W/m/K reflecting the high

clay content. These values correspond to the lower range of thermal conductivities measured in the sedimentary formations as well as in the Permocarbon and crystalline rocks in Weiach.

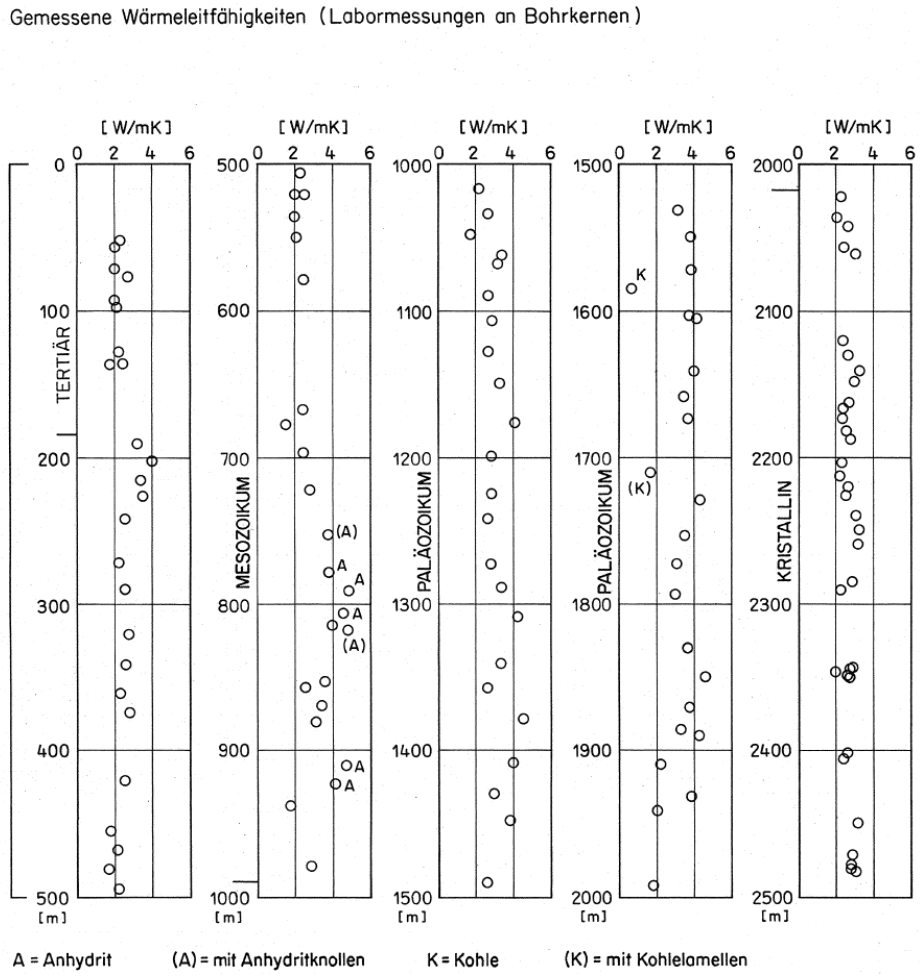

Fig. 2-5: Profiles of thermal conductivities measured in core samples from the Weiach borehole (Nagra 1988).

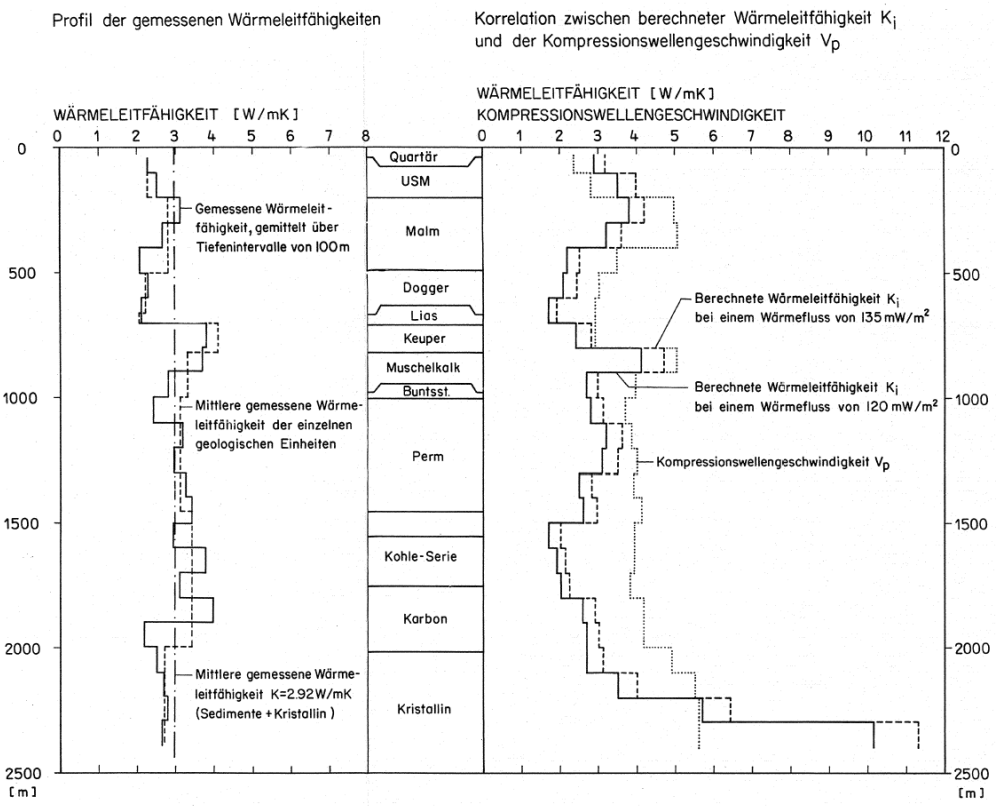

Fig. 2-6: Profile of thermal conductivities averaged per 100 m increments and compared to the corresponding stratigraphic profile in Weiach. The correlation to compressional wave velocity is shown on the right side (Nagra 1988).

Additional measurements of thermal conductivity have been carried out on Opalinus Clay core samples from the Benken borehole (Nagra 2000) indicating an anisotropy of the thermal conductivity (Table 2-1). The anisotropy is attributed to small-scale bedding planes with high-conductive quartz-rich depositions affecting the heat flow in the horizontal direction and low-conductive clay-rich depositions controlling flow in the vertical direction (Nagra 2000, Nagra 2001).

An additional set of heat conductivity values is provided by means of model calibrations (Ollinger and Baujard 2012). These were carried out in 1D models using the lithostratigraphic profile of the Weiach borehole. Calibrated values using three different approximations of the stratigraphy are shown in Figure 2-7. Similar to the core sample measurements, thermal conductivity of the Opalinus Clay is approximately 2.0 W/m/K which corresponds to the lowest value in the profile of Weiach.

Specific heat capacity is typically provided only by laboratory measurements under controlled conditions, as transient conditions allowing the quantification of heat storage are difficult to monitor in the field and to reproduce accurately with models. Measurements of specific heat capacity are carried out using calorimeters assuming that the heat capacity of the solid matrix and the heat capacity of the pore water are linearly scaled with porosity to the total heat capacity of the saturated rock sample. Such measurements are available for Opalinus Clay samples taken from the Benken borehole (Nagra 2000) and are given in Table 2-2.

Tab. 2-1: Measurements of specific heat capacity of Opalinus Clay in the Benken borehole.

Probe	Probe depth [m bgl] from	to	C, matrix [J/g,K]	C, water [J/g,K]	C, total [J/g,K]	C, total [J/Kg,K]
Op1	559.93	560.04	0.78	4.18	0.93	930
Op2	574.94	575.06	0.72	4.18	0.88	880
Op3	589.52	589.62	0.75	4.18	0.90	900
Op4	596.00	596.10	0.79	4.18	0.94	940
Op5	603.93	604.00	0.80	4.18	0.94	940
Op6	609.50	609.58	0.77	4.18	0.92	920
Op7	615.00	615.10	0.79	4.18	0.94	940
Op8	620.02	620.09	0.76	4.18	0.91	910
Op9	636.00	636.10	0.80	4.18	0.94	940
Op10	650.04	650.14	0.79	4.18	0.94	940

Tab. 2-2: Measured thermal conductivity, temperatures and temperature gradients in the Opalinus Clay (Nagra 2001).

	OPA Thermal Conductivity [w/m/K]	OPA top temperature [°C]	OPA bottom temperature [°C]	Temperature gradient [°C/m]
Weiach	2.0	32	39	0.044
Benken	Upper OPA (538-625 m): 3.2 (horizontal) 1.8 (vertical)	30	38	0.043
	Lower OPA (625-652 m): 2.0 (horizontal) 1.3 (vertical)			

					muT	muT	Lamda [W/mK]		
Strati	Strati	Strati	Litho	id	Top	Bottom	Weiach 1	Weiach 2	Weiach 3
Quartär	Pleistozän		Kies	1	0	30	3.2	3.2	3.2
			Kies	2	30	37	3.2		
Tertiär	USM		Siltstein Tonstein	3	37	59	3.2		
			Siltstein Sand	4	59	151	3.25		
			Siltstein Tonstein	5	151	177	3.1		
	Bohnerz		Tone	6	177	186	3		
Malm	Kimmeridgian		Mikrit	7	186	221	4.2	3.83	3.48
			Kalk	8	221	230	3.8		
			Mikrit	9	230	271	4.1		
			Mergel	10	271	276	2.9		
			Kalk + Pelmikrit	11	276	296	3.9		
			Kalkmergel	12	296	316	3.5		
	Oxfordien		Mikrit	13	316	336	3.7		
			Mikrit	14	336	380	3.8		
			Kalkmergel	15	380	390	2.74		
		Effinger Sch.	Mergel	16	390	426	2.61	2.61	
		Effinger Sch.	Mergel	17	426	478	2.6		
Dogger	Callovien		Kalk und Tonmergel	18	478	483	2.6	2.54	2.27
	Bathonien		Tonmergel	19	483	491	1.94		
			Tonmergel	20	491	520	2.6		
	Bajocien		Kalkmergel	21	520	536	2.8		
			Mergel	22	536	540	2.6		
	Aalenian		Tonsteine siltig	23	540	554	2.4		
		Opalinuston	Tonmergel	24	554	600	2.2	2.08	
		Opalinuston	Ton	25	600	666	2		
Lias	Toracien		Tonmergel	26	666	678	2.4	2.56	2.56
	Pl. + Sine		Tonsteine	27	678	694	1.75		
	Het.		Kalke	28	694	704	2.45		
Keuper			Dolomitmergel	29	704	719	2.65		
			Tonmergel	30	719	724	2.82		
			Dolomit	31	724	727	2.94		
			Tonsteine	32	727	739	2.4		
	Gipskeuper		Tonsteine mit Anhydritknollen	33	739	760	2.6		
			Tonsteine	34	760	781	2.4		
			Tonsteine mit Anhydritlagen	35	781	803	2.8		
			Anhydrit	36	803	814	3.39		
	Lettenkeuper		Dolomit	37	814	820	3		
Ob.			Dolomit	38	820	857	3.5	3.61	3.29
Muschelkalk			Dolomit und Kalk	39	857	888	3.7		
Mitt.			Dolomit	40	888	898	3.74		
Muschelkalk			Tonsteine	41	898	906	4.23		
			Tonsteine und Anhydrit	42	906	930	4.4		
			Anhydtit und Dolomit	43	930	945	2		
Unt.			Kalk und Tonmergel	44	945	950	2	2.43	
Muschelkalk			Tonsteine	45	950	973	2.27		
			Tonsteine	46	973	982	2.78		
Buntsandstein			Sandsteine	47	982	992	2.69		
Perm	Saxonien		Ton und Siltstein	48	992	1058	2.4	2.56	2.56
	und Thurgien		Breccie	49	1058	1086	3.8		
			Ton/Sandstein/Breccie	50	1086	1170	3.5		
	Autunien		Siltstein/Sandstein	51	1170	1252	3.3		
			Tonsteine	52	1252	1270	2.78		
			Sandsteine	53	1270	1285	3		
			Mergel	54	1285	1297	3.44		
			Konglomerat	55	1297	1310	3.43		
			Mergel	56	1310	1340	2.6		
			Ton/Siltstein/Sandstein	57	1340	1360	3.07		
			Sandsteine	58	1360	1388	3.2		
			Sandsteine	59	1388	1424	3.2		
			Ton/Siltstein/Sandstein	60	1424	1474	2.5		
Karbon	Stephanien		Sandsteine	61	1474	1551	2.6		
			Tonsteine	62	1551	1585	1.5		
			Konglomerat	63	1585	1612	1.8		
			Ton/Siltstein	64	1612	1650	2		
			Ton	65	1650	1663	2		
			Ton	66	1663	1675	2		
			Sandsteine	67	1675	1694	3		
			Ton	68	1694	1723	1.4		
			Ton	69	1723	1738	2.3		
			Ton	70	1738	1752	2.1		
			Ton/Sandstein/Konglomerat	71	1752	1840	2.7		
	Stephanien		Sandstein/Konglomerat	72	1840	1951	3		
			Ton/Sandstein	73	1951	2020	2.3		
Kristallin			Gneis, kataklastisch	74	2020	2060	3.3	4.04	4.04
			Gneis, wenig Störzone	75	2060	2250	4		
			Gneis	76	2250	2482	4.2		

Fig. 2-7: Calibrated values of thermal conductivity for Weiach (from AXPO 2011).

2.3.3 Temperature data

Temperature profiles measured in boreholes can be compared with heat transport models and used for calibrating uncertain parameters such as thermal rock properties and base rock heat flow. Such calibrations were performed for thermal conductivity of the hydrogeological units considered in the Nördlich Lägern local model and are discussed in Section 3. Figure 2-8 shows different temperature measurements from the Weiach borehole described in detail in Nagra (1988). These can be summarized as follows:

- Bottom Hole Temperature (BHT) measurements are carried out at the bottom of the borehole after drilling. BHT measurements are typically distorted by thermal effects from the drilling fluid and have to be corrected accordingly. Four BHT measurements are available from Weiach at depths of approximately 800 (Keuper), 1750 (Permocarbon) and 2050 and 2450 m in the Crystalline.
- Hydraulic Test (HT) data can provide temperature measurements during hydraulic testing of certain depth intervals. One HT temperature measurement is available from Weiach at a depth of 988 m in the lower Muschelkalk formation.
- High Resolution Temperature (HRT) logs are carried out with HRT-sensors and can provide precise continuous logs of temperature-depth profiles depending on the measurement increments. These may vary from centimeters to meters. 46 HRT measurements are available from Weiach.

The HRT- profile in Figure 2-8 indicates an increase of temperature below the Opalinus Clay (depths > 666 m) above the average linear gradient, suggesting a low thermal conductivity of the Opalinus Clay combined with high thermal conductivities in the underlying Keuper formation that lead to heat accumulation and geothermal gradient build-up below the Opalinus Clay. This is corroborated by the core sample measurements indicating a low thermal conductivity of the Opalinus Clay. A similar change in the geothermal gradient is observed at 1500 m depth due to coal layers in the carboniferous Coal-Series that have relatively low thermal conductivities of approximately 0.6 W/m/K (Nagra 1988).

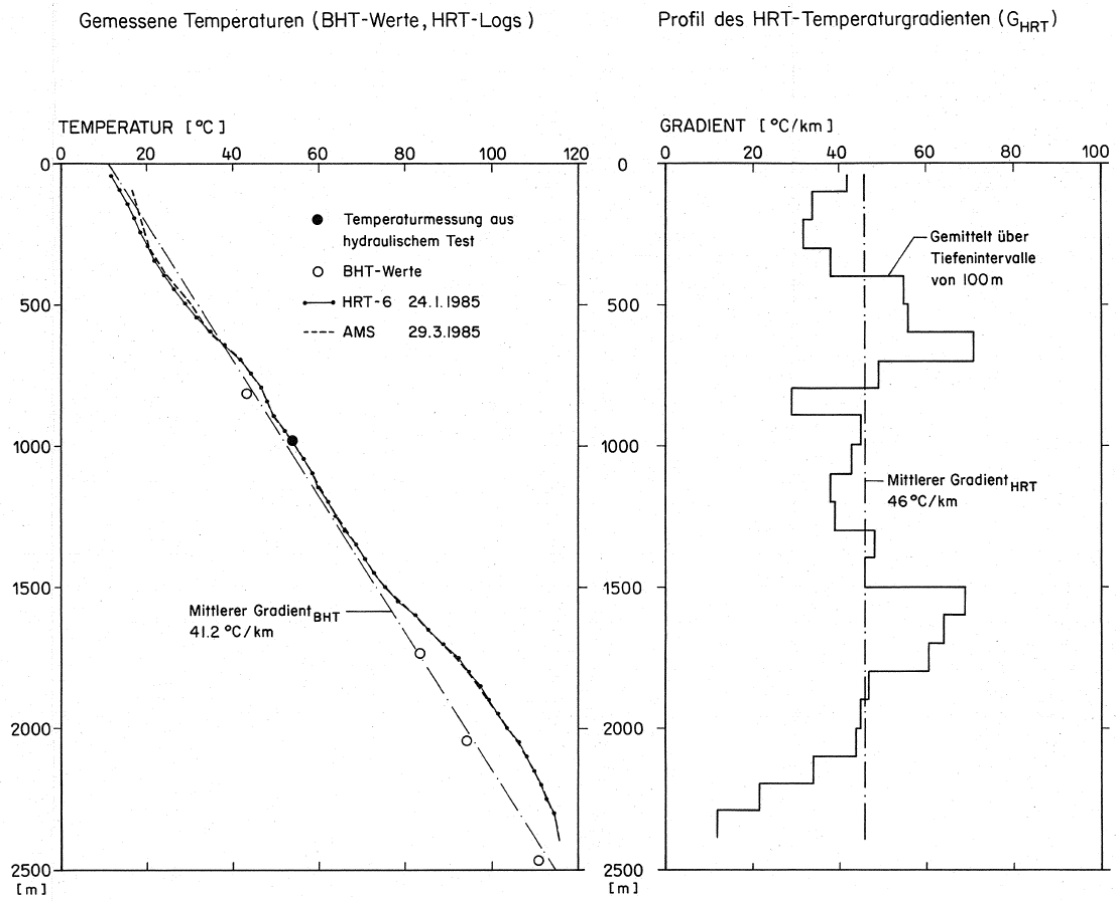

Fig. 2-8: Temperature profiles measured in the Weiach borehole (left). Temperature gradients have been derived in 100-m gradients (right). From Nagra (1988).

The temperature profiles measured in deep investigation boreholes are not only controlled by current geothermal state conditions (basal heat flow, surface temperature, thermal conductivity profile, groundwater flow) but also by historic climate changes. During ice ages, the subsurface temperature distribution was influenced by the reduced temperatures at ground surface. The depth of influence of a typical glacial-interglacial cycle has been estimated e.g. by Clauser et al. (1997) to be at around 1000-1500 m bgl. The decline of temperatures at the beginning of an ice age, and the subsequent rise of temperatures at the end of it, are important input parameters for any thermal or coupled thermo-hydraulic modelling. Most important here are the maximum and minimum temperatures reached during the glacial-interglacial cycle as well as the duration of these cycles. In this report, the temperature differences and durations of the last ice age in northern and central Europe have been used as a first order approximation of the possible temperatures and durations during such cycles. Fig. 2-9 shows that surface temperatures generally range between 10° C and 0° C at the surface. Temperatures below 0° C, in which extended permafrost areas could have developed, have only been reconstructed for (relatively) short periods of time of not more than 5000 a (see Fig. 2-9).

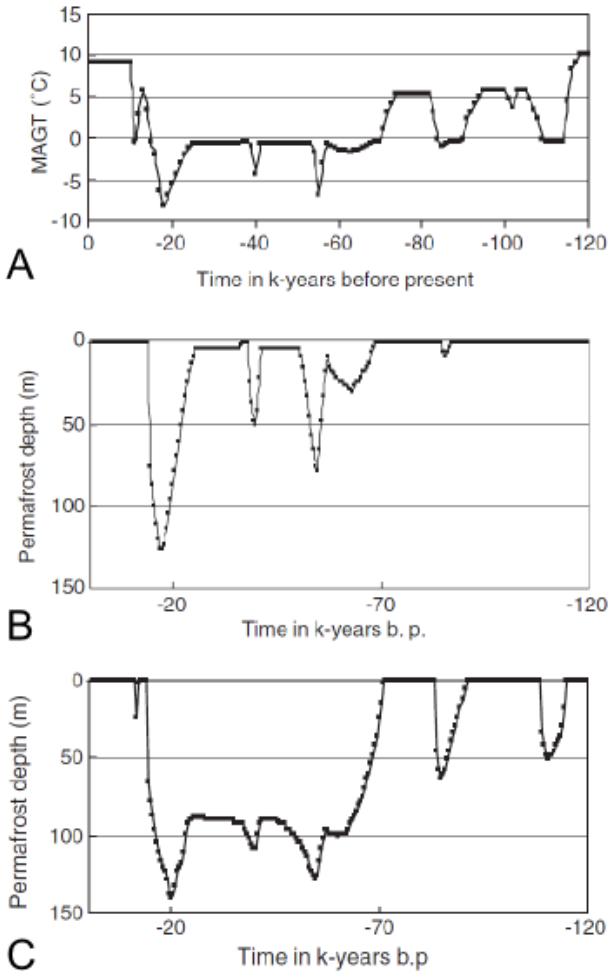

Fig. 2-9: A) Temperature-Time curve for the last 120000 for central Europe estimated from reconstructed Mean Annual Ground surface Temperatures (MAGT). B) Permafrost depth for the Weichselian based on the reconstructed MAGT-curve shown in A. C) Permafrost depth for the Weichselian based on the MAAT-curve. This curve is presented as an approximation for the case of vegetation-poor, elevated areas with little snow cover in winter. (modified from Deslile et al. 2003).

While permafrost obviously greatly influences the hydrogeological conditions of an area (e.g. preventing recharge) so does the thawing of previously frozen ground. Among other processes, the development of thermokarst may change the hydrogeology of the modelled area during thawing. The changes of the hydrogeology related to freezing and thawing of water cannot adequately be represented in the used modelling software, hence temperatures below 0° C have not been included in the respective variant of the thermo-hydraulic model presented in this report. In the context of the analyses presented in this report this is appropriate since the permafrost layer never reaches the proposed repository site nor the surrounding host rocks. Permafrost depths have been reconstructed in northern and central Europe for the last ice age by Deslisle et al. 2003 (see Fig. 2.9) showing that even during the time periods with the lowest temperatures, permafrost depth is always less than 150 m.

3 Modeling of Thermo-Hydraulic Evolution in Nördlich Lägern

Modeling the thermo-hydraulic evolution in the siting region Nördlich Lägern is performed step-wise by initially developing the hydraulic model and consequently extending it to include thermal effects. The hydrogeological model is introduced in Section 3.1 with more a detailed description available in Luo et al. (2014). Based on this model, effects of heat transport are implemented as described in Section 3.2. In Section 3.3 the necessary steps for calibrating the model are discussed. Finally predictions on the thermo-hydraulic evolution of the region are provided through analyses of different scenarios in Section 3.4.

3.1 Development of the hydrogeological model

The numerical analysis of the hydrogeological conditions is carried out on different scales. First, a regional hydrogeological model is developed for northern Switzerland incorporating the stratigraphy and spatial elevations of the Mesozoic sedimentary rocks, as well as local and regional faults and hydrologic conditions. The regional model is consequently broken down to form so-called local models which are used for the description and analyses of hydrogeological conditions in the individual siting regions (Luo et al. 2014).

3.1.1 Hydrogeological regional model

The regional hydrogeological model was constructed using a geological model (GeoMod 2012.1, see Gmünder et al. 2013) incorporating all available sources of information such as seismic lines, boreholes, outcrops etc. (see Figure 3-1). Based on this geological model, a regional hydrogeological model was established. The layers included in the regional hydrogeological model are (from top to bottom): the Quaternary, OSM, OMM, USM, the Malm Aquifer, the Effingen Member, the "upper" Dogger, the Hauptrogenstein Aquifer[1], the "lower" Dogger, the Opalinus Clay, the clay-rich Lias and Keuper, the Keuper Aquifer, the Gipskeuper, the Muschelkalk Aquifer and the basal Anhydritgruppe. The Hauptrogenstein and Keuper aquifers were not part of the geological model but were constructed using simple thickness rules in the hydrogeological model. The regional fault system implemented in the geological model had to be simplified in the regional hydrogeological model to limit the complexity of the mesh generation process and simulations. For this purpose, the faults were rotated vertically with the center of rotation being at the top surface.

[1] The model domain Nördlich Lägern lies within a transition zone where the Hauptrogenstein Formation in the west is replaced by the Klingnau Formation in the east. Within the model domain, only the Spatkalke of the Hauptrogenstein Fm. occur. Nevertheless, the equivalent hydrogeological unit in the model Nördlich Lägern is called Hauptrogenstein so that terminology is consistent with the regional geological model though, strictly speaking, it comprises the Spatkalke of the Hauptrogenstein Formation.

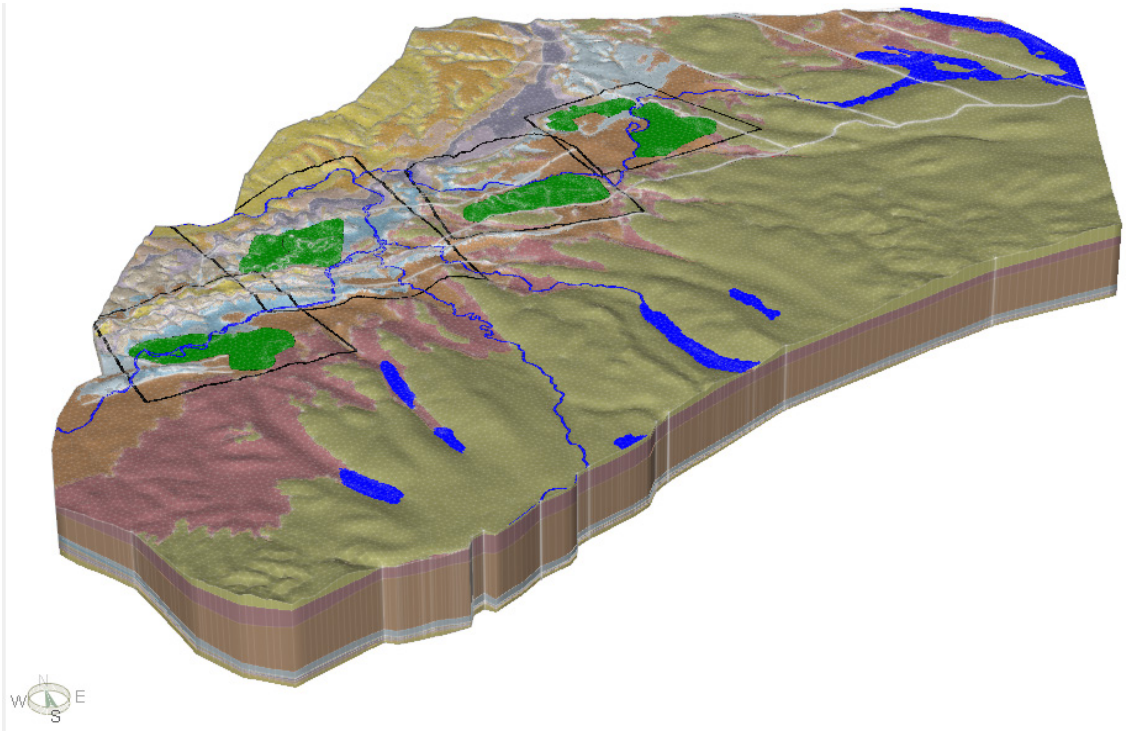

Fig. 3-1: 3D hydrogeological model including all relevant horizons and layers. Black lines delineate the boundaries of the local-scale hydrogeological models JS, JO, NL and ZNO-SR, green polygons resemble possible siting regions, white lines are trace lines of regional faults implemented in the model. Only the major rivers and lakes (blue) are shown (the model contains all major rivers and their tributaries). 2x vertical exaggeration, Quaternary cover not shown (Luo et al. 2014).

3.1.2 Hydrogeological local model Nördlich Lägern

Based on the regional geological model, four local hydrogeological models were constructed corresponding to the siting regions Jura-Südfuss (Local Model JS), Jura Ost (Local Model JO), Nördlich Lägern (Local Model NL), Zürich Nordost and Südranden (Local Model ZNO-SR).

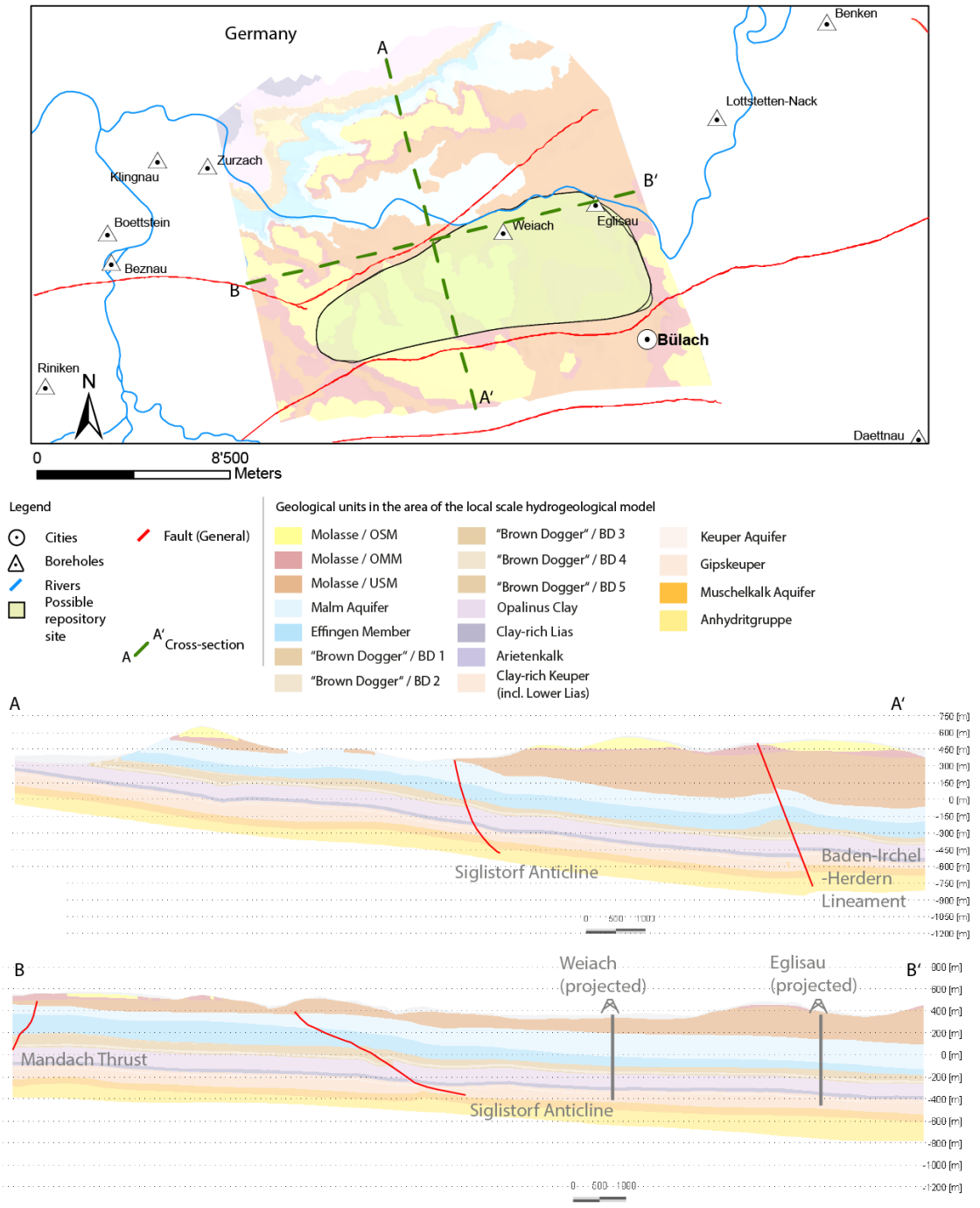

Fig. 3-2: Overview of the local model Nördlich Lägern (from Luo et al. 2014).

In order to construct these models, the different local models were cut out of the regional geological model and the same hydrogeological units as in the regional hydrogeological model (see Figure 3-1) were constructed. In addition, several hydrogeological units were added to ensure an adequate representation of the local groundwater flow conditions. Thus, local aquifer systems/potentially transmissive units were implemented within the Dogger, Lias and Keuper units. These units have all been included using thickness rules (usually the minimum and maximum thickness of the layer and the distance to the next layer already existing in the geological model). The added hydrogeological units in the local model NL were the Keuper Aquifer (constant thickness of 10 m), the Arietenkalk (constant thickness of 3 m) and the so called 'Brown Dogger 5' (BD5), a thin layer of constant thickness (10 m) just above the Opalinus Clay. The resulting model is shown in Figure 3-2. This model, including the inclined Mandach Thrust, Baden-Irchel-Herdern Lineament and the Siglistorf Anticline, is used for the model calibration and the final simulations (see Figure 3-5).

Hydraulic head boundary conditions were assigned at the vertical model boundaries corresponding to the Muschelkalk Aquifer, Keuper Aquifer and Malm Aquifer, taken from the hydrogeological regional model (see Gmünder et al. 2013; and Lueo et al. 2013 for further details). At the Quaternary- and Tertiary aquifers, fixed hydraulic heads were assigned at the river network delineated on the model surface.

Tab. 3-1: Stratigraphic units, model layers and corresponding hydraulic properties in the *FEFLOW_3D* model.

Formation	Stratigraphic Unit	Hydrogeological Unit	Kh [m/s]	Kv [m/s]
Quaternary	Quaternary	Quaternary	1e-4	1e-4
Tertiary	Tertiary - OSM	Molasse - OSM	2e-8	2e-11
	Tertiary - OMM	Molasse - OMM	1e-6	1e-9
	Tertiary - USM	Molasse - USM	5e-9	2e-11
Malm	Villigen Fm.	Malm Aquifer	1e-6	1e-6
	Wildegg Fm./ Effingen Member	Effingen Member	1e-11	1e-12
Dogger	Upper Dogger	'Brown Dogger 1'	1e-11	1e-12
	Spatkalke (Hauptrogenstein Fm.)	'Brown Dogger 2'	1e-8/2e-7	1e-8/2e-7
	Klingnau Fm.	'Brown Dogger 3'	5e-13	1e-13
	Passwang Fm.	'Brown Dogger 4'	5e-12	1e-12
	Sissach Member	'Brown Dogger 5'	5e-10	5e-10
	Opalinus Clay	Opalinus Clay	1e-13	2e-14
Lias	Upper Lias	Clay-rich Lias	1e-13	1e-13
	Arietenkalk	Arietenkalk	1e-12	1e-12
	Lower Lias	Clay-rich Keuper (incl. lower Lias)	1e-12	1e-12
Keuper	Upper Mittelkeuper			
	Sandsteinkeuper/ Stubensandstein/ Gansinger Dolomit	Keuper Aquifer	1e-9	1e-9
	Gipskeuper	Gipskeuper	1e-14	1e-14
Muschelkalk	Upper Muschelkalk	Muschelkalk Aquifer	5e-8/1e-5	5e-8/1e-5
	Middle Muschelkalk	Anhydrit	1e-10	1e-10

3.2 Implementation of heat flow model

The numerical investigations of the thermo-hydraulic evolution in the siting region Nördlich Lägern were developed in two steps. In a first step, 1D and 3D model calibrations were performed for the site-specific stratigraphy, hydrogeological setting and model considerations used in the NL local model. In a second step, calibrated values were implemented in the 3D flow and heat transport local-scale model for Nördlich Lägern. The applied methodology is summarized in the following:

Model calibrations

Initially, a 1D vertical column is used for calibrating formation thermal conductivities to the HRT- temperature profile given in Nagra (1988) using the iTOUGH2 program (Finsterle 1999). This model will be referred to as *iTOUGH2_1D*. The vertical column is constructed based on lithostratigraphic logs from the Weiach borehole. The lithostratigraphic facies in the detailed profile from Weiach (Section 2.2 / Figure 2-3) are described with the stratigraphic classification illustrated in Figure 3-3, making it consistent with previous work on calibrating formation thermal conductivities (AXPO 2011). The column is discretized by 1-m elements, extending from the surface and respective top of the Tertiary sediments to the crystalline basement at a depth of 2482 m. Pressure boundary and initial conditions are represented by a hydrostatic pressure distribution so that advection does not contribute to heat transport. A constant temperature of 10 °C is assigned at the top. The heat flow assigned to the bottom of the column is equal to 120 mW/m² (Nagra 1988, pp.134). The column sides are treated as no-flow boundaries (Figure 3-3). The simulation is run until steady-state conditions are reached.

The next step includes implementing a 1D column model for heat transport in FEFLOW, aiming to provide comparison to the *iTOUGH2_1D* model and validation between the two codes based on the predicted temperature profiles. This model will be referred to as *FEFLOW_1D*. The same stratigraphic units are taken into account, as shown in Figure 3-3, however the column comprises only 8 layers spanning from the surface to a depth of 991 m that corresponds to the base of the Muschelkalk and respective top of the Permo-crystalline. Pressure distribution is hydrostatic using hydraulic head boundary and initial conditions. Temperature at the top is fixed at 10 °C while heat inflow at the bottom is set to 120 mW/m² or 10368 J/m²/d. The thermal conductivity values assigned to the formations are those obtained from the calibration runs with *iTOUGH2_1D*.

Once calibration and validation with the 1D models is complete, the calibrated thermal conductivities are assigned to the corresponding stratigraphic units in the 3D local model for Nördlich Lägern (Luo et al. 2014) for simulating flow and heat transport with FEFLOW. This model is denoted here as *FEFLOW_3D* and comprises 19 layers spanning from the surface to the base of the Muschelkalk. The model is initially run without taking any thermal effects into account. The resulting head distribution (Figure 3-4) is then used as an initial condition for a second simulation that includes heat transport. For this, a constant uniform heat inflow of 120 mW/m² or 10368 J/m²/d is prescribed at the bottom of the model and a constant temperature of 10 °C is assigned at the surface. The simulation is run to steady-state. Two sets of thermal conductivities are used for the simulations: (1) the values obtained from the 1D calibration, and (2) values from lab measurements carried out with core samples from the Weiach borehole (Figure 3-3). Furthermore, different numerical aspects are tested in the model. The temperature profiles predicted for Weiach with these model runs are then compared to the 1D profiles from *iTOUGH2_1D* and *FEFLOW_1D* as well as from the HRT- measurements.

In a final step, the revised *FEFLOW_3D* model is used for modeling the thermo-hydraulic evolution in the siting region Nördlich Lägern. The mesh, boundary and initial conditions used are shown in Figure 3-4. The formation thermal conductivities and numerical approaches used for the simulations are obtained from the previous steps of model calibration.

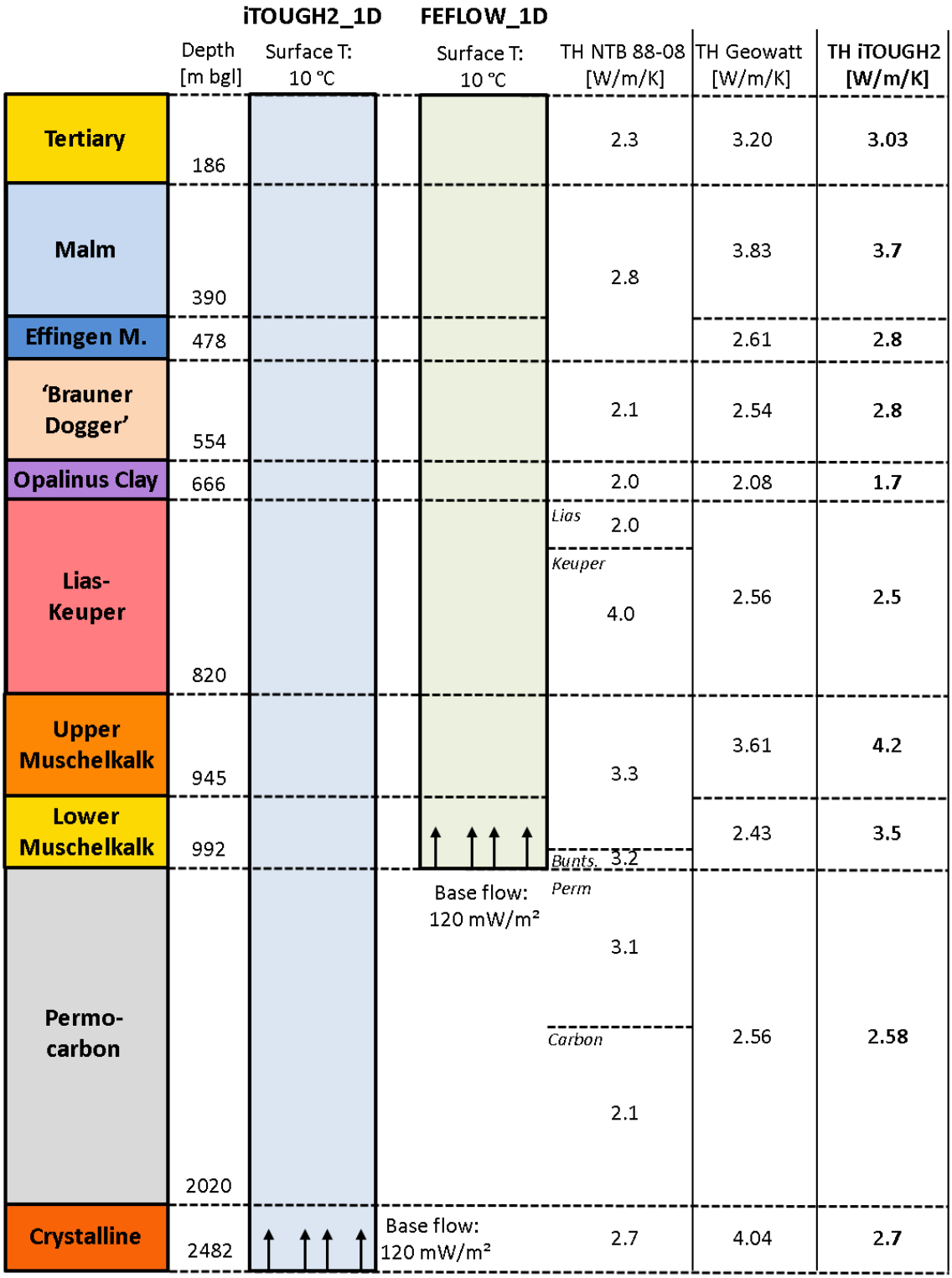

Fig. 3-3: Stratigraphic profile used for the 1D calibration models. The columns denoted with *iTOUGH2_1D* and *FEFLOW_1D* indicate the vertical extent and boundary conditions used in the models. A comparison of different values of formation thermal conductivity is given on the right side: formation averages based on core measurements (Nagra 1988), calibrated values from AXPO (2011), and calibrated values with iTOUGH2.

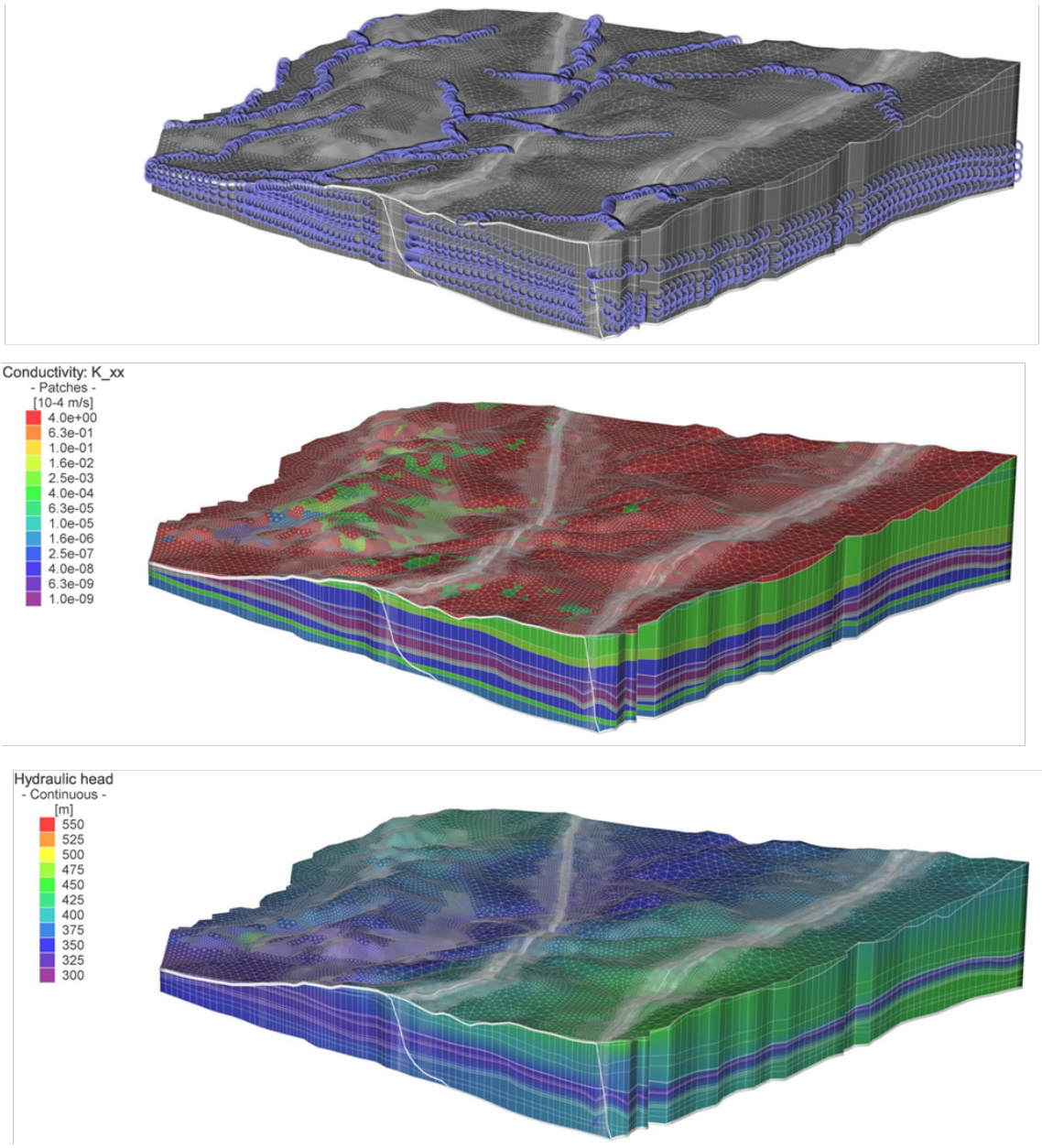

Fig. 3-4: Fixed-head boundary condition nodes (top), hydraulic conductivity (middle) and the resulting head distribution used as initial condition (bottom) for the heat transport simulations with *FEFLOW_3D*. These boundary conditions are taken from the corresponding hydrogeological model detailed in Luo et al. (2014).

3.3 TH-model Calibrations

The calibrations of the TH-model are first carried out with 1D numerical simulations. Consequently, calibrated parameters are introduced in the 3D model and tested for their ability to re-produce the temperature measurements available from Weiach.

3.3.1 1D model calibrations

The thermal conductivities were calibrated to the HRT- temperature profiles using two approaches in the *iTOUGH2_1D* model. The first approach (case *iTOUGH2_1D_r1*) neglects any natural emission of heat from the geological formations. The second approach (case *iTOUGH2_1D_r2*) takes into account a natural heat emission equal to 5e-04 mW/m³ (Ollinger and Baujard 2012) that is assigned as a heat source term uniformly across the entire vertical column. Figure 3-5 shows the resulting temperature profiles and the calibrated thermal conductivity values of the different formations using the two approaches. The comparison indicates that a good agreement to the measured temperature profile is feasible with both approaches, as the fitted thermal conductivities do not show significant differences. The increase of temperatures at the depth of the Opalinus Clay is also captured by the calibration runs, yielding low thermal conductivity values for the Opalinus Clay (1.7 and 1.9 W/m/K in *iTOUGH2_1D_r1* and *iTOUGH2_1D_r2*, respectively). This agrees with thermal conductivity values determined for Opalinus Clay in Benken, Weiach and Riniken (see Table 2-2). A comparison of thermal conductivities fitted with *iTOUGH2_1D_r1* to the average formation thermal conductivities measured in cores from Weiach is given in Figure 3-3. More details on the calibration parameters and results are given in the Appendix. Additional analyses related to the length of the 1D model used for transient- and steady-state calculations are also provided in the Appendix.

	iTOUGH2_1D_r1 TC [W/m/K]	*iTOUGH2_1D_r2* TC [W/m/K]
Tertiary	3.0	3.0
Malm	3.7	3.7
Effingen M.	2.8	2.8
'Brown Dogger'	2.8	2.8
Opalinus Clay	1.7	1.9
Lias-Keuper	2.5	2.6
Upper Muschelkalk	4.2	4.5
Lower Muschelkalk	3.5	3.5
Permocarbon	2.6	2.7
Crystalline	2.7	2.7

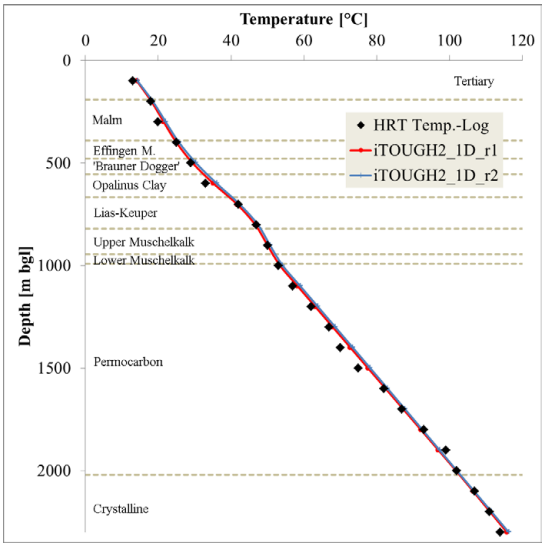

Fig. 3-5: Calibrated temperature profiles and thermal conductivities with the iTOUGH_*1D* model.

In general, the two main mechanisms that contribute to heat transport through porous media are convection and conduction. Heat convection occurs when heat is transported by advective flow of groundwater. Heat conduction occurs through diffusive transport of heat owing to a temperature gradient. Heat transport is thus controlled by the interplay between these mechanisms, with convection dominating in advective flow systems and conduction dominating in diffusion-controlled transport systems. Finite element methods used for modeling heat transport typically use upwinding techniques in order to smooth steep temperature gradients and prevent numerical oscillations (see i.e. FEFLOW white papers, vol.1). These techniques improve numerical stability but also introduce numerical dispersion, so that a comparison is

typically performed to indicate possible advantages or discrepancies. For this, the thermal conductivities fitted with *iTOUGH2_1D_r1* were implemented in the *FEFLOW_1D* model to test two numerical approaches. The first approach employed full upwinding in the finite element discretization of the flow and heat transport problem and is tested with a simulation run referred to as *FEFLOW_1D_r1*. The second approach employed a shock-capturing scheme (Diersch 1998) and is tested with simulation *FEFLOW_1D_r2*. The full upwinding approach smoothens temperature gradients in all directions significantly increasing numerical stability but also numerical dispersion. On the other hand, the shock-capturing approach stabilizes convection-dominated transport processes through a non-linear anisotropic damping factor applied in the neighborhood of sharp fronts or discontinuities, removing oscillations about a front with significantly reduced artificial dispersion away from it. Model runs employing these two approaches provided the steady-state temperature profiles that are illustrated in Figure 3-6. The same figure provides a comparison to the *iTOUGH2_1D_r1* case and the HRT measurements. In the case of a 1D heat transport problem, fully upwinding and shock capturing deliver the same temperature profile in steady-state. With lateral gradients neglected and hydrostatic pressure assigned to the 1D column, heat convection is restricted to flow related to density and viscosity changes with temperature and therefore remains negligible compared to heat transport through conduction. Effects associated with the numerical treatment of convective transport are therefore minimized. The conduction of heat results in a monotonic increase of temperature from 51.4 °C at the bottom to 10 °C at the surface.

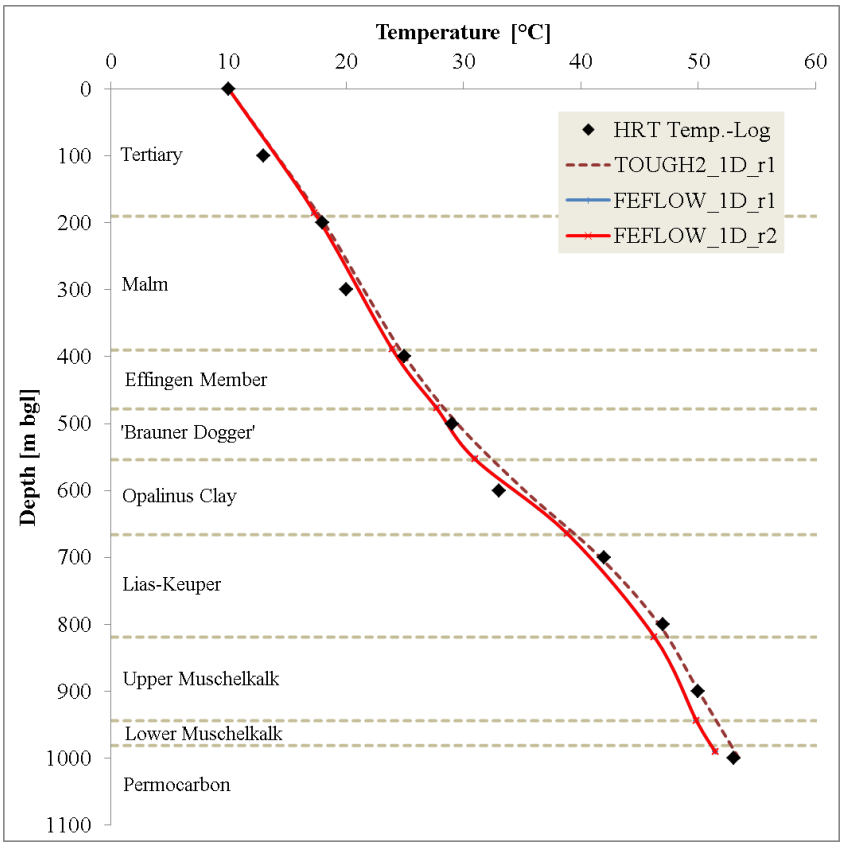

Fig. 3-6: Comparison of the HRT- measured temperature profile to profiles predicted with *iTOUGH_1D* model and the *FEFLOW_1D* model using the fully upwinding and shock capturing schemes.

3.3.2 3D model calibrations

In addition to the 1D calibrations, the impact of thermal properties and model parameters on the thermo-hydraulic behavior have to be investigated with a three-dimensional model in order to capture possible effects associated with the heterogeneities, gradients, lateral and cross-formational flows imposed in the NL local model. To minimize the computational effort of large 3D model simulations, the *FEFLOW_3D* model was used to simulate steady-state temperature profiles for the following combinations of input:

FEFLOW_3D_r1: thermal conductivity fitted with *iTOUGH2_1D_r1*, fully upwinding scheme.
FEFLOW_3D_r2: thermal conductivity measured in core samples, fully upwinding scheme.
FEFLOW_3D_r3: thermal conductivity fitted with *iTOUGH2_1D_r1*, shock capturing scheme.
FEFLOW_3D_r4: thermal conductivity measured core samples, shock capturing scheme.

Figure 3-7 shows temperature profiles predicted with the *FEFLOW_3D* model. It is observed in all simulations that the temperature of 10 °C remains almost constant through the base of the tertiary layer at approximately 59 m depth. This behavior relates to advective flow of water recharging and discharging through the high-permeable top layers. Heat reaching the Tertiary and Quaternary is thus quickly dissipated through the surface boundary conditions. This effect was not captured in the 1D models that neglect lateral groundwater gradients.

Comparison of the first two runs to the HRT- temperature data indicates that the general pattern of the temperature profile is reproduced by the simulations; however, in some cases the simulated values deviate from the measurements by up to 5.5 °C. The fully upwinding numerical scheme combined with the calibrated conductivity (*FEFLOW_3D_r1*) results in a temperature profile similar to the measurements but shifted to lower values. This is due to convective flow through the Tertiary and Quaternary that in principle shifts the effect of the 10 °C boundary condition to the base of these layers. Applying the shock capturing scheme (*FEFLOW_3D_r3*) improves the results and reduces deviations from the measurements to 1-2 °C. The measured thermal conductivity combined with fully upwinding (*FEFLOW_3D_r2*) delivers a temperature profile that in general agrees with the HRT measurements, however produces maximum deviations of 4 °C in the Opalinus Clay and the 'Brown Dogger'. Using the shock capturing scheme, the predicted values increase so that the corresponding deviation from the measurements increases to 5.5 °C.

In conclusion, thermal conductivity was successfully calibrated to the HRT- profile with iTOUGH2 and consequently used to verify simulations carried out in FEFLOW. As explained in Section 3.2, this input from the calibrations will be used for simulating the regional thermo-hydraulic evolution in Nördlich Lägern.

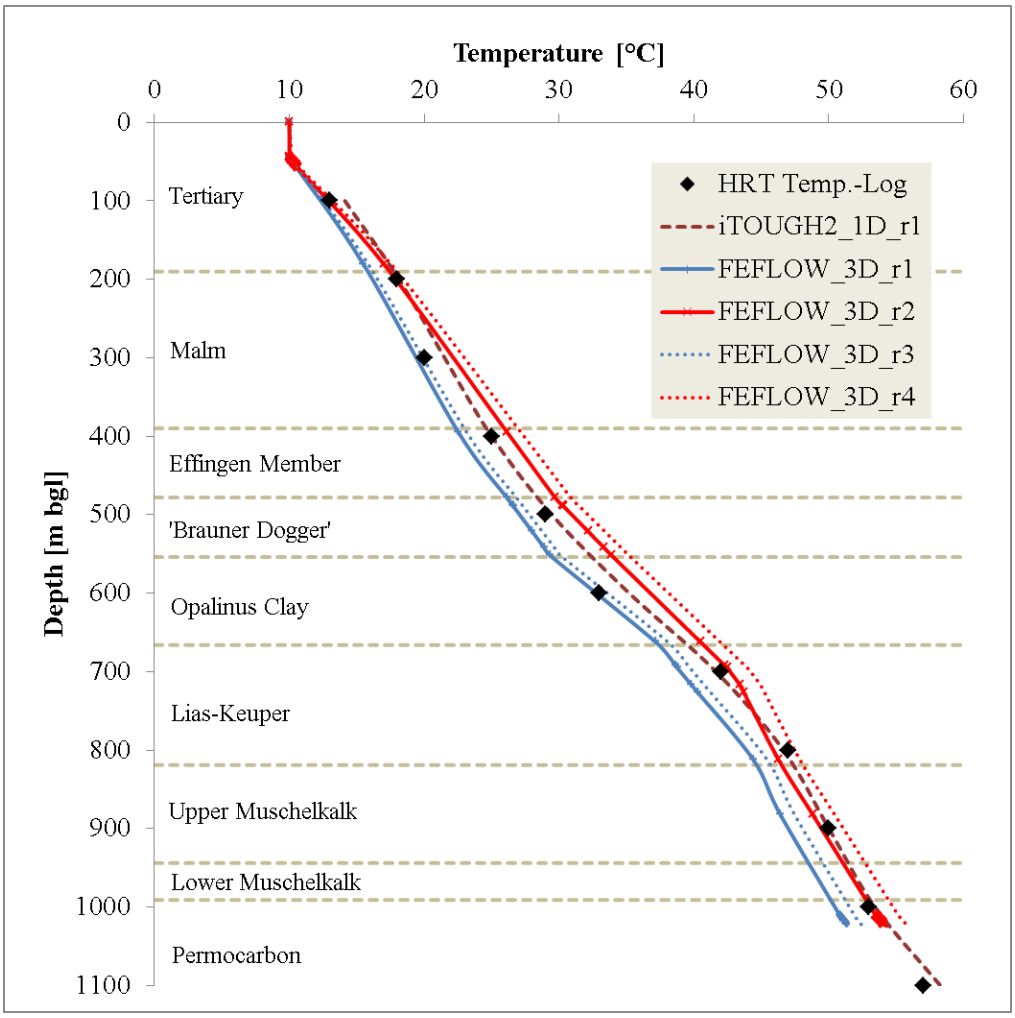

Fig. 3-7: Comparison of the HRT- measured temperature profile to profiles calibrated with the *iTOUGH_1D* model (*iTOUGH_1D_r1*) and predicted with the *FEFLOW_3D* model using fitted thermal conductivity combined with fully upwinding (*FEFLOW_3D_r1*), measured thermal conductivity combined with fully upwinding (*FEFLOW_3D_r2*), fitted thermal conductivity combined with shock capturing (FEFLOW_*3D_r3*) and measured thermal conductivity combined with shock capturing (*FEFLOW_3D_r4*).

3.4 TH-model Runs

Based on the developed model approaches and inputs described in the previous sections, the thermo-hydraulic evolution in Nördlich Lägern is investigated with a reference simulation and four simulation variants.

Model runs

The model considerations and input parameters established with the calibration and preliminary simulations in 1D and 3D were transferred to the model to investigate the thermo-hydraulic evolutions in the area with the help of a reference simulation and four simulation variants.

- Reference case: a simulation of the steady-state condition corresponding to basal flow of 120 mW/m² and 10 °C at the surface (Chapt. 3.4.1).
- Variant 1: a simulation assuming low hydraulic conductivity of the regional faults (Chapt. 3.4.2).
- Variant 2: a simulation taking into account variations of temperature at the surface related to ice age periods (Chapt. 3.4.3).
- Variant 3: a simulation assuming spatially variable basal heat flow at the bottom of the model (Chapt. 3.4.4).
- Variant 4: a simulation taking into account the natural emission of heat from geological formations (Chapt. 3.4.5).

3.4.1 Reference case

The reference simulation is carried out based on the initial and boundary hydraulic conditions provided by the *FEFLOW_3D* model (Figure 3-4). The boundary conditions for heat transport are assigned according to the considerations described in sections 3.2 and 3.3 with fixed heat inflow at the bottom boundary and fixed temperature at the surface. The calibrated thermal conductivities are used as input for the heat transport using the shock-capturing FE scheme.

Figure 3-8 depicts the simulation results in terms of the three-dimensional distribution of temperature representing steady-state conditions. The minimum temperature corresponds to 10 °C prescribed at the model surface. In general, temperature increases with depth and increasing distance from the surface respective decreasing distance to the Muschelkalk base. The maximum temperature of 76 °C is observed in the lowermost layer at the southeast corner of the NL local model that also corresponds to the greatest depth below the ground surface. Figure 3-8 also delineates the Opalinus Clay formation layer, which spans a wide range of depths from approximately 1300 m below ground surface in the south to 100 m below ground surface in the north, with some outcrops appearing at the northeast part of the model. Temperatures in the Opalinus Clay are accordingly low in the north where the formation is closer to the surface and increase southwards with increasing formation depth. Values vary between 10 °C at the outcrop at the northwest corner of the model, and approximately 20-30 °C in the northeast, 30-45 °C in the southwest and 50-65 °C in the southeast corresponding to the greatest formation depth. In Weiach, temperatures at the base and top of the Opalinus Clay are 38 and 30 °C, respectively.

Figure 3-9 shows cross-sections of temperature distributions spanning the NL local model in the north-south (NS), north/northeast-south/southwest (NNE2SSW_B), and west-east (WE3) directions, respectively. The plots show isolines spanning parallel to the surface elevation, indicating that surface morphology affects the temperature distribution even in the deeper parts of the model (i.e. 500 m below ground surface in cross-section WE3). Along the NS and NNE2SSW_B cross-sections, temperatures in the Opalinus Clay vary from 12 °C to 50 °C depending on the formation depth. Along the WE3 cross-section, the Opalinus Clay dips gently and eastwards, resulting in formation temperatures ranging between 26 °C and 54 °C.

Figure 3-9 further illustrates the disruption of the Opalinus Clay layer by the major fault zones that cross the model domain from east to west and northeast to west. These introduce local discontinuities of the formation at an elevation of -100 m and -500 m in the NS and NNE2DDW_B cross-section, respectively. In the reference simulation, the fault zones were assumed to be highly conductive with a constant and isotropic hydraulic conductivity of

1.0e-7 m/s. The simulation results show that the discontinuities in the geological formations and corresponding thermal properties slightly disturb the temperature isolines spanning through the fault zones, especially in the deeper sections corresponding to the Opalinus Clay and the underlying layers. The isoline depression indicates enhanced heat flow by convective heat transport through the high-permeable fault zones.

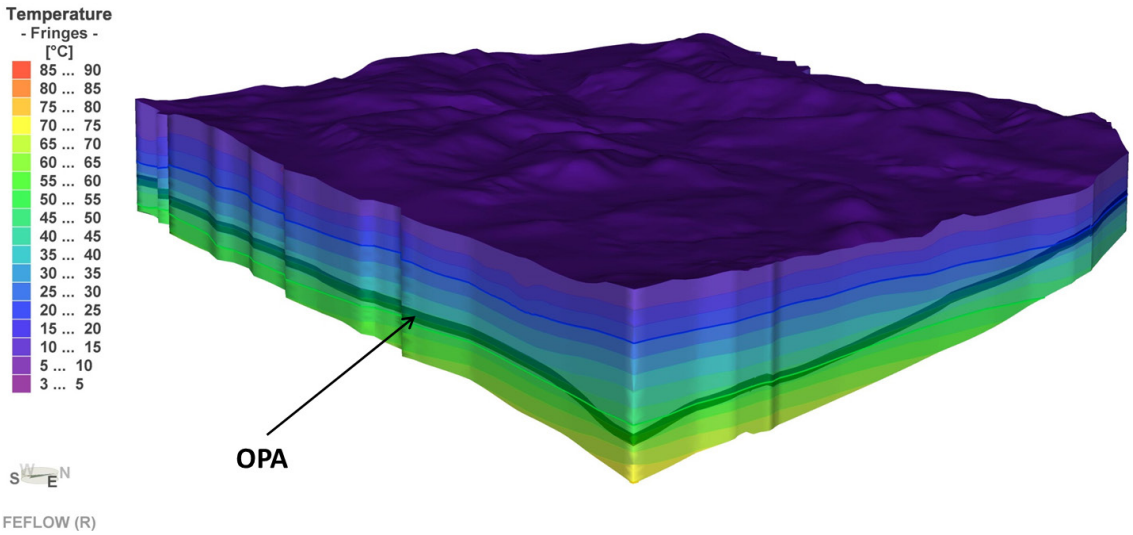

Fig. 3-8: Reference simulation: temperature distribution predicted with the *FEFLOW_3D* model. The shaded layer indicates the Opalinus Clay formation.

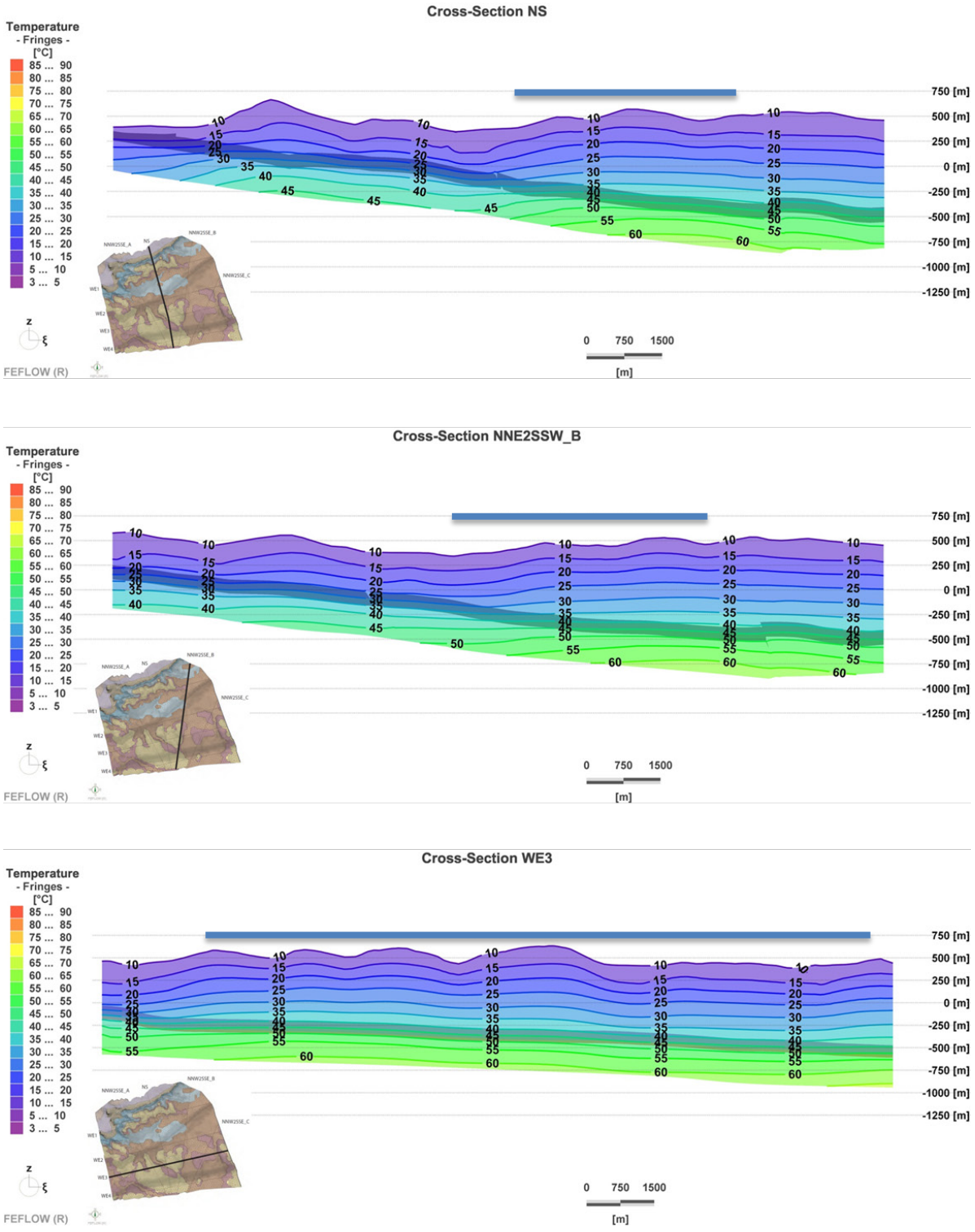

Fig. 3-9: Reference simulation: cross-sectional temperature distribution in the North-South (NS), North/NorthEast-South/SouthWest (NNE2SSW_B) and West-East (WE3) direction. The shaded layer indicates the Opalinus Clay formation. Blue bar indicates the aproximate position of the siting region.

3.4.2 Variant 1

The interplay between convective and conductive heat transport implies that the existence of pathways with high contrasts in conductivity may alter the flow regime and therewith determine the mechanisms for heat transfer. In steady-state conditions, low-conductive formations are expected to enhance the influence of the fixed-temperature boundary condition at the surface affecting the underlying layers through conduction. On the other hand, high-conductive formations allow for more convective flow of heat through the fixed-inflow boundary condition at the bottom.

Simulation Variant 1 aims to quantify the role of regional fault structures on heat migration and the overall geothermal conditions in the area. Regional faults of high conductivity may impact the geothermal regime by forming preferential pathways for heat transport driven by advective groundwater flow. To investigate the impact of such preferential pathways, a simulation with the *FEFLOW_3D* model was performed for comparison to the reference simulation. In the reference simulation the hydraulic conductivity of regional faults was set to 1.0e-7 m/s, enhancing hydraulic gradients through the faults crossing the geological layers. In this simulation Variant 1, the inclined regional faults were assumed to be low-conductive by assigning a hydraulic conductivity equal to 1.0e-15 m/s. Similar to the reference simulation, hydraulic conductivity of the faults was assumed isotropic.

Figure 3-10 shows the resulting temperature distributions for cross-sections NS, NNE2SSW_B and WE3. Compared to the reference simulation (Figure 3-9 and Figure 3-8), formation temperatures predicted with Variant 1 are generally higher. This effect diminishes in the north and appears more pronounced in the southern part of the local model where temperatures in Variant 1 were locally higher by as much as 5 °C. Decreasing the fault permeability limits advective groundwater flow and thus convective heat transport through the faults, increasing the temperature in the deeper parts of the model. The difference in the results between the reference case and Variant 1 indicate the local contribution of convection in heat transport occurring through the fault zones. At the lowermost part of the NS cross-section in the vicinity of the fault, the highest temperatures reach 65 °C in Variant 1 (Figure 3-10), compared to 60 °C in the reference case (Figure 3-9). A more detailed comparison between the reference case and simulation Variant 1 in terms of temperature isolines in the vicinity of the fault zone in cross-section NS is given in Figure 3-11. It is observed that whereas temperature isolines span unperturbed through the fault in Variant 1, they are perturbed by the fault zone in the reference case, indicating the effect of enhanced heat transport by convection. On the other hand, the effect is insignificant away from the fault zone; in the vicinity of the Weiach borehole, temperatures from Variant 1 at the top and bottom of the Opalinus Clay are 30 and 38 °C, respectively, which is the same as in the reference simulation.

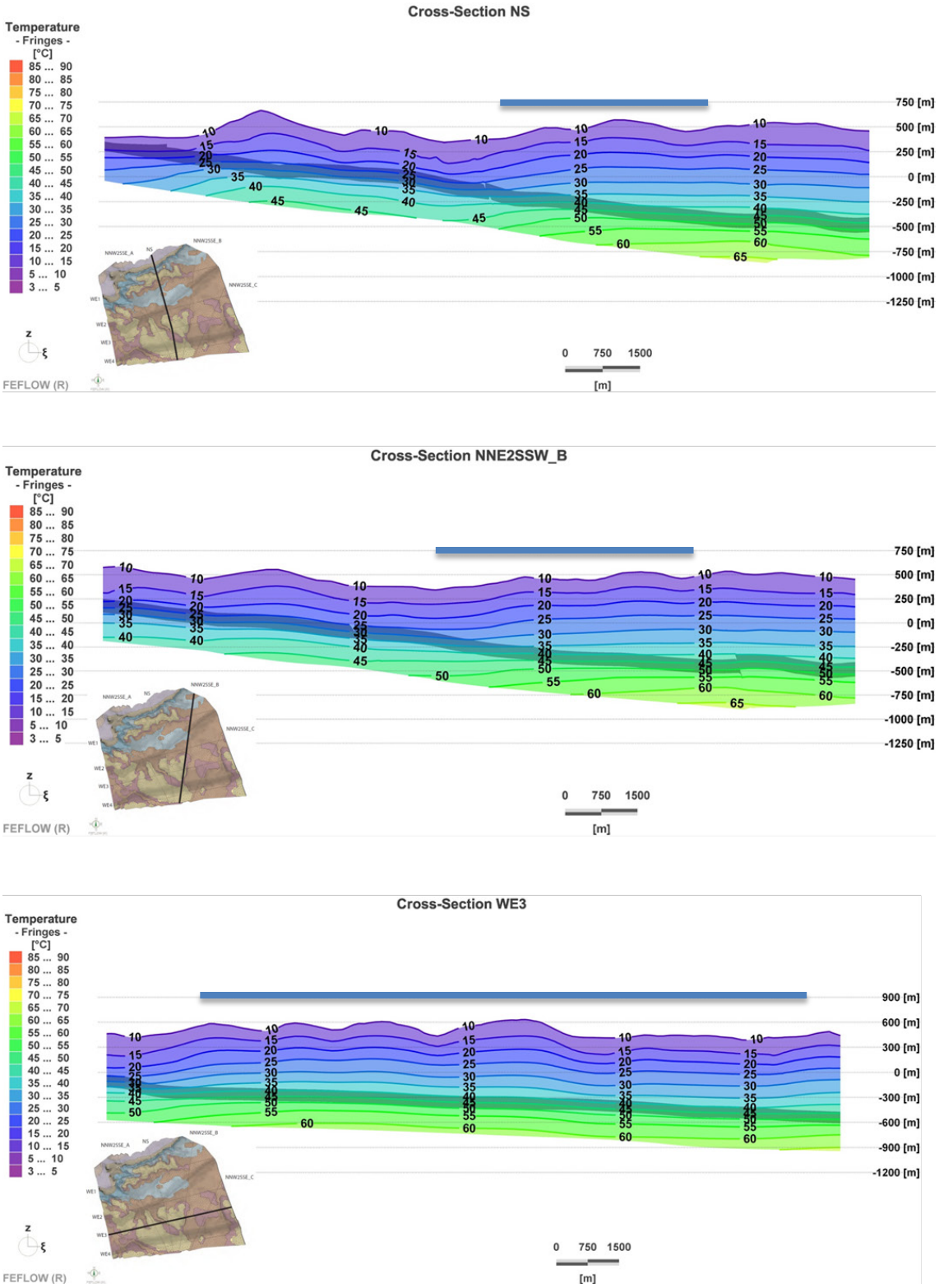

Fig. 3-10: Simulation Variant 1: cross-sectional temperature distribution in the North-South (NS), North/NorthEast-South/SouthWest (NNE2SSW_B) and West-East (WE3) direction. The shaded layer indicates the Opalinus Clay formation. Blue bar indicates the aproximate position of the siting region.

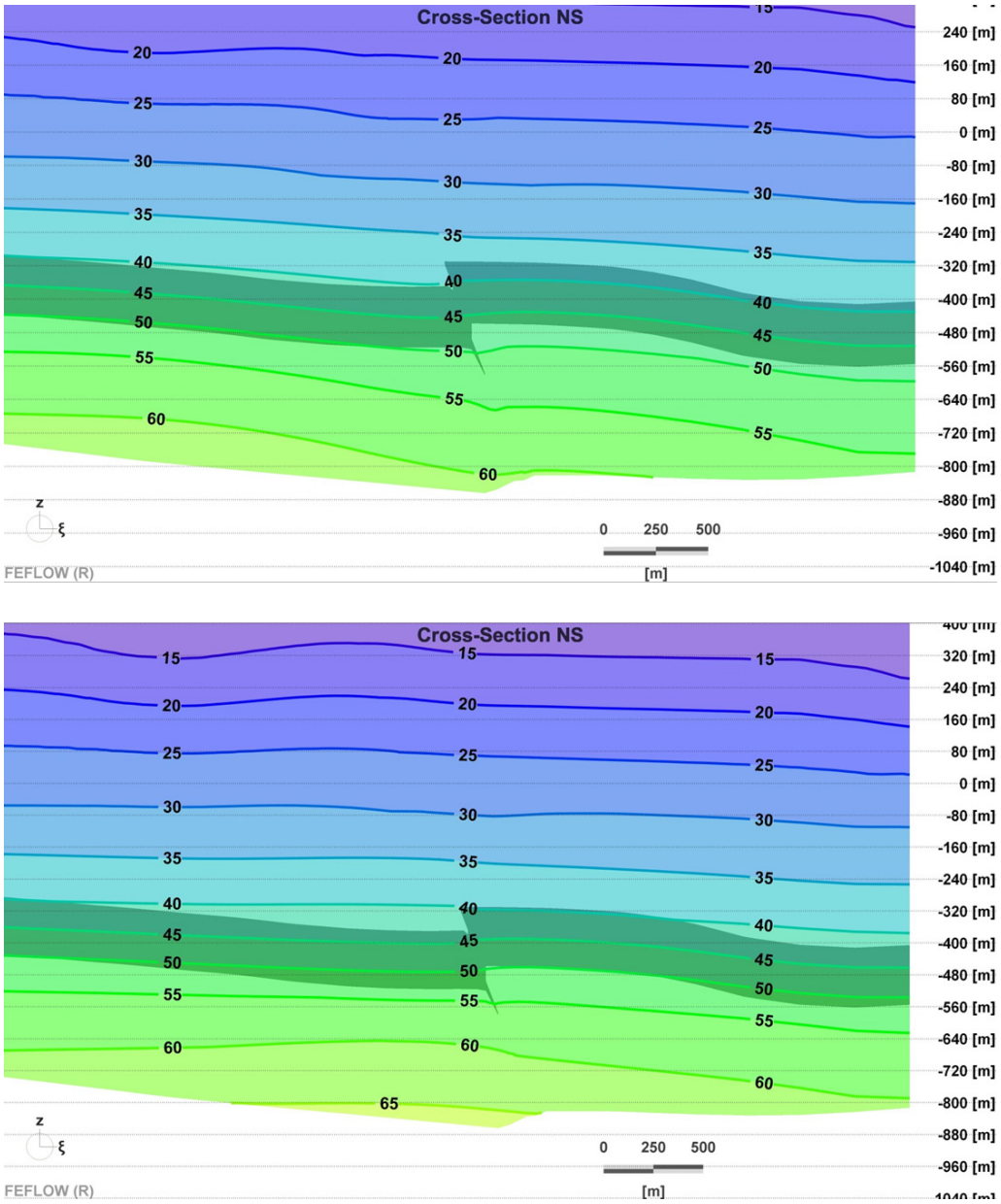

Fig. 3-11: Detailed comparison of temperature isolines between the reference case (top) and simulation Variant 1 (bottom) in cross-section NS. Isolines of 45, 50 and 55 °C appear perturbed in the reference case, whereas span undisturbed through the fault zone in Variant 1.

3.4.3 Variant 2

The second variant aims to quantify the impact of temperature variations at the ground surface corresponding to a generic glacial/interglacial cycle. Aspects of the transient behavior associated with the depth of the heat flow boundary condition were analyzed separately with a 1D model and are discussed in the Appendix. The aim of this simulation was not to reproduce past glacial cycles or to predict future cycles but to allow a general quantification of temperature variations during glacial cycles. As explained in chapter 2.3.3, the used modeling software is not capable of adequately representing permafrost, therefore temperatures below 0°C have been excluded from the implemented tT-path shown in Fig. 3-12. The ice age is implemented

following steady-state conditions resulting from a surface temperature of 10 °C, which constitutes the initial state for the onset of the ice age. An estimation of surface temperature variations taking into account an ice-age over a period of 100,000 years is shown in Fig. 3-12. This temperature variation is implemented by means of successive simulations of the *FEFLOW_3D* model where temperature- and head distributions extracted from the final time-step of each simulation is used as the initial condition for the next simulation having different temperature boundary conditions. These simulation steps correspond to the following ice age phases respectively boundary conditions:

- Steady-state corresponding to surface temperature of 10 °C.
- Phase 1 (-100,000 to -78,000 years): surface temperature of 11 °C over a period of 22,000 years (simulation *FEFLOW_3D_case2.1*).
- Phase 2 (-78,000 to -58,000 years): surface temperature of 6.3 °C over a period of 20,000 years (simulation *FEFLOW_3D_case2.2*).
- Phase 3 (-58,000 to -18,000 years): surface temperature of 3 °C over a period of 40,000 years (simulation *FEFLOW_3D_case2.3*).

In general, the temperature distribution in the 3D model domain is determined by the interplay between the basal heat flow prescribed at the bottom boundary and the surface temperature corresponding to the ice age period. Figure 3-13 shows profiles of temperature vs. depth obtained at the location of the Weiach borehole and at different times of the implemented ice age periods. Initially, surface temperature corresponds to 10 °C, the maximum temperature of approximately 55 °C is observed at the Muschelkalk bottom. The first change of surface temperature variation taken into account corresponds to 11 °C and therefore does not introduce significant changes compared to the initial steady-state condition. In the second phase, surface temperature is reduced to 6.3 °C causing a shift of the temperature profile to lower temperatures wherein temperature changes delay with increasing depth. Deviations from the initial condition are thus observed later at the bottom of the model with temperature decreasing to 52.8 °C and 51.4 °C after 10,000 and 20,000 years, respectively. During the third phase, surface temperature is further decreased to 3 °C, consequently causing a maximum temperature shift at the bottom to 49.3, 48.0 and 47.2 °C after 10,000, 20,000 and 40,000 years, respectively.

Figure 3-14 also shows a comparison of the corresponding temporal evolution of temperature at the base of the Muschelkalk to the temperature evolution at the finite element mesh nodes corresponding to the top of the Opalinus Clay formation in Weiach. Temperature at the top of the Opalinus Clay reaches a maximum of 31 °C at the end of Phase 1 followed by a decrease to 27.1 and 23.3 °C at the end of Phase 2 and Phase 3, respectively. An illustration of temperature change relative to the initial state (Figure 3-14, right) indicates that the simulated system approaches, though not entirely, thermal steady-state during each of the ice age periods. At the end of the three phases, temperature at the top of the Opalinus Clay decreases by 2.7%, 10.2% and 22.9% compared to the initial temperature, respectively.

Figure 3-15 shows plots of temperature distributions at the end of the three ice age phases for the selected cross-section spanning the NL local model in the North-South direction. It shows that temperature isolines shift parallel (and approximately parallel to the surface) for each shift of temperature applied at the surface. Additional cross-sections of temperature in the west-east and north/northwest-south/southeast direction after the completion of Phase 3 of the ice age are given in Figure 3-16. In the NS and NNE2SSW_B cross-sections, temperatures in the Opalinus Clay range from 4 °C to 45 °C depending on depth. In the WE3 cross-section temperatures in the Opalinus Clay vary between 20 °C and 46 °C.

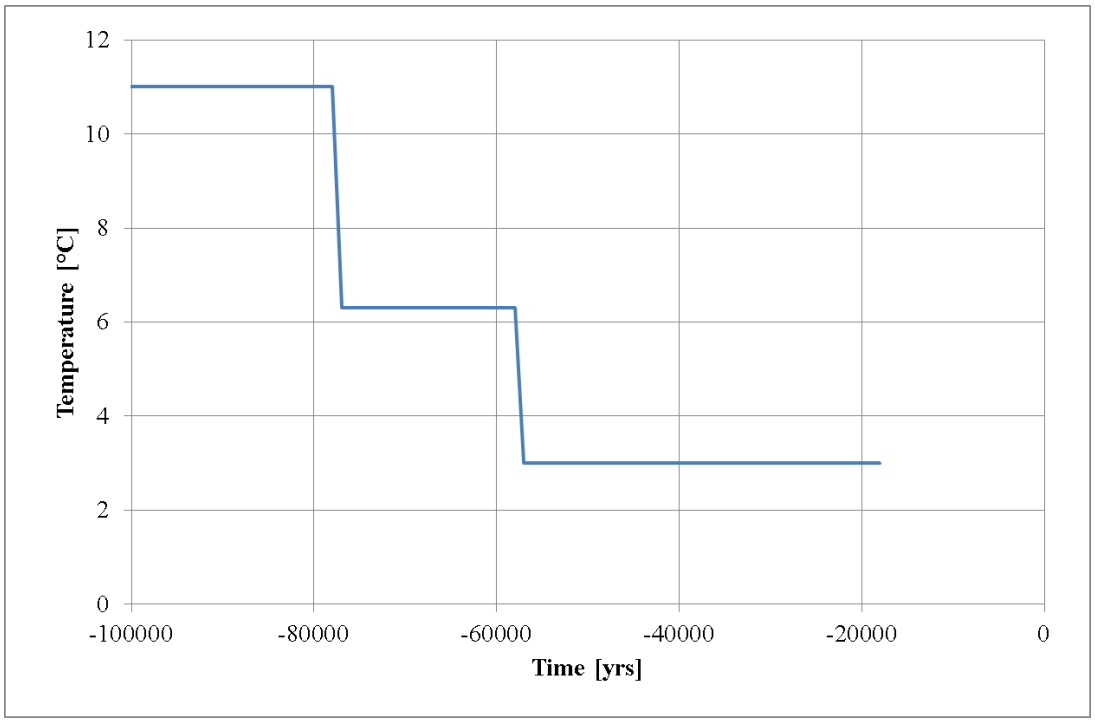

Fig. 3-12: Simulation Variant 2: surface temperature variations during an ice-age cycle of 100,000 years. The original curve (see Fig. 2-9A) has been simplified to exclude temperatures where permafrost may develop.

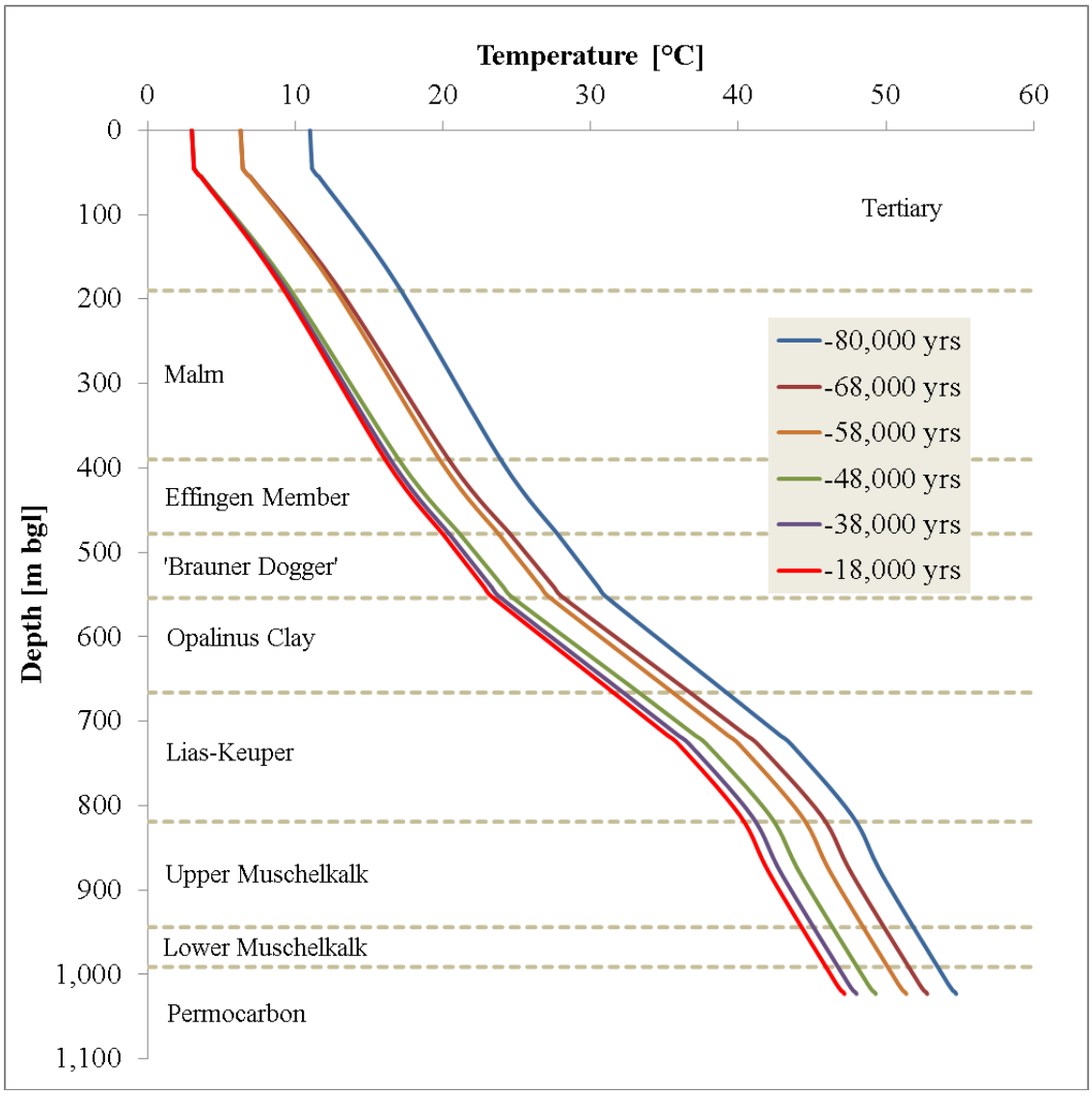

Fig. 3-13: Simulation Variant 2: predicted temperature profiles at the location of the Weiach borehole during Phase 1 (top), Phase 2 (middle) and Phase 3 (bottom) of the ice-age period.

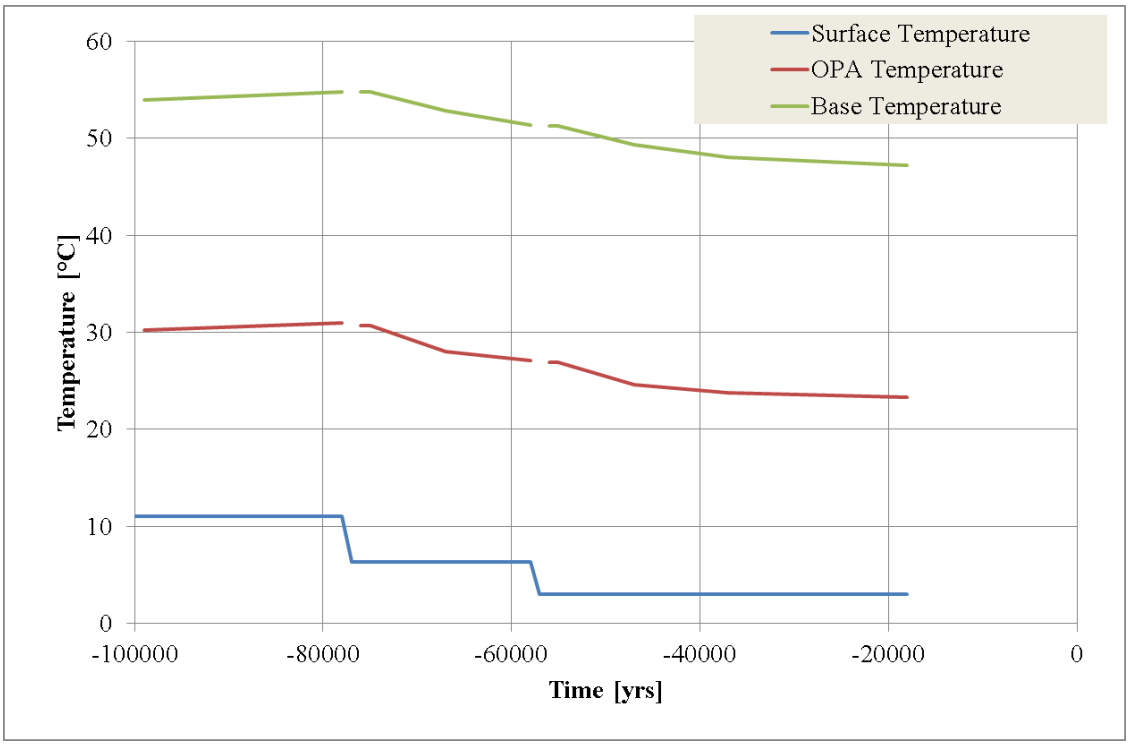

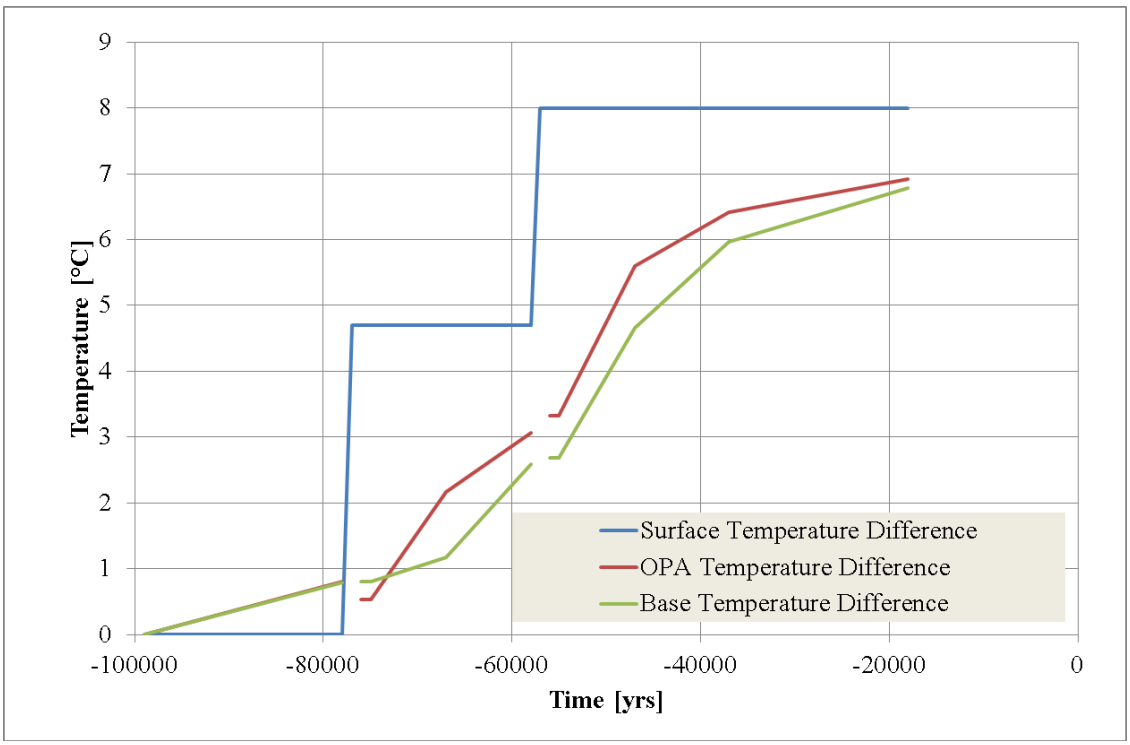

Fig. 3-14: Simulation Variant 2: comparison of surface temperature variation to temperature evolution in the Opalinus Clay (top) and at the base of the Muschelkalk respective base of the model domain (bottom).

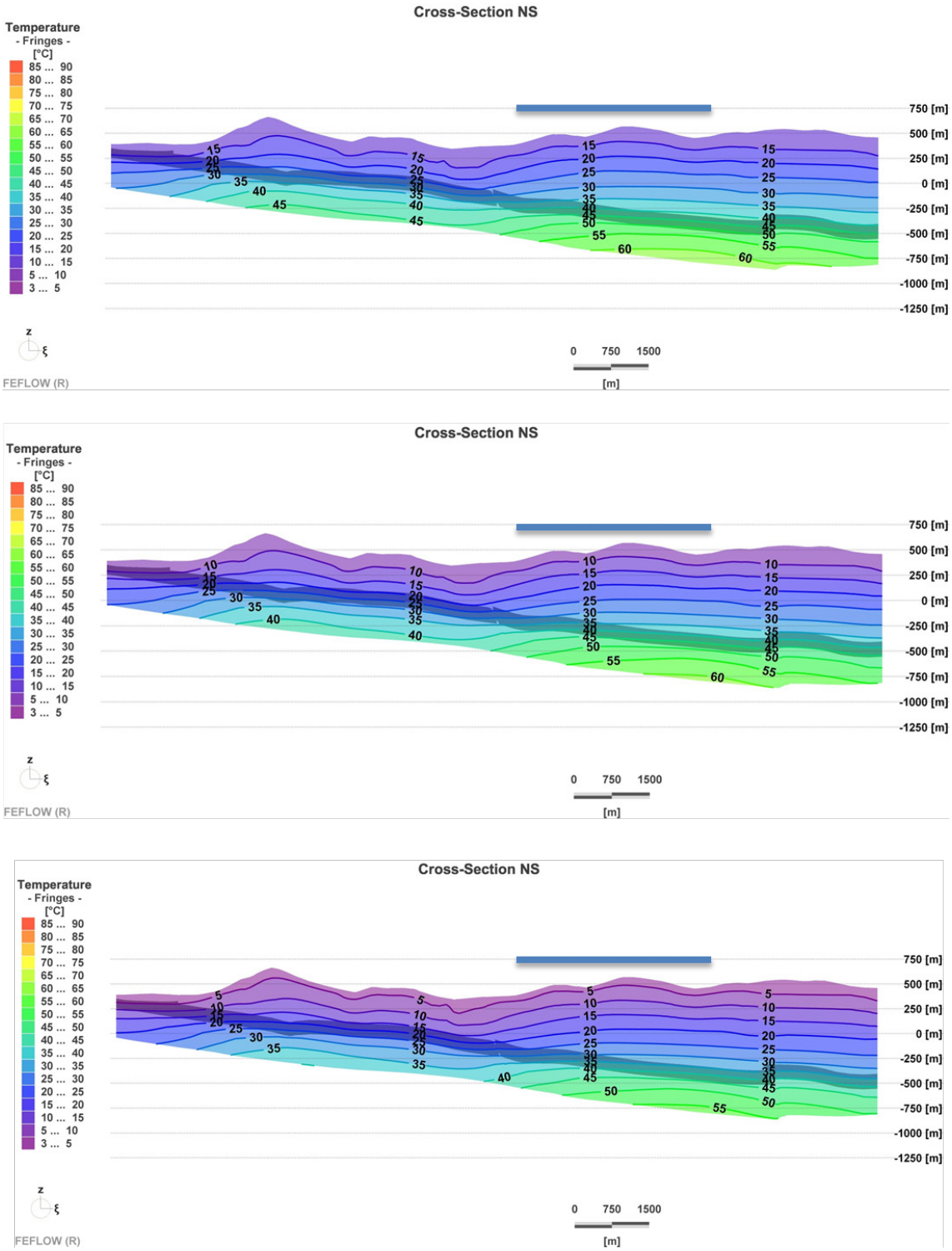

Fig. 3-15: Simulation Variant 2: cross-sectional temperature distribution in the North-South (NS) direction at the end of Phase 1 (top), Phase 2 (middle) and Phase 3 (bottom) of the ice age period. The shaded layer indicates the Opalinus Clay formation. Blue bar indicates the aproximate position of the siting region.

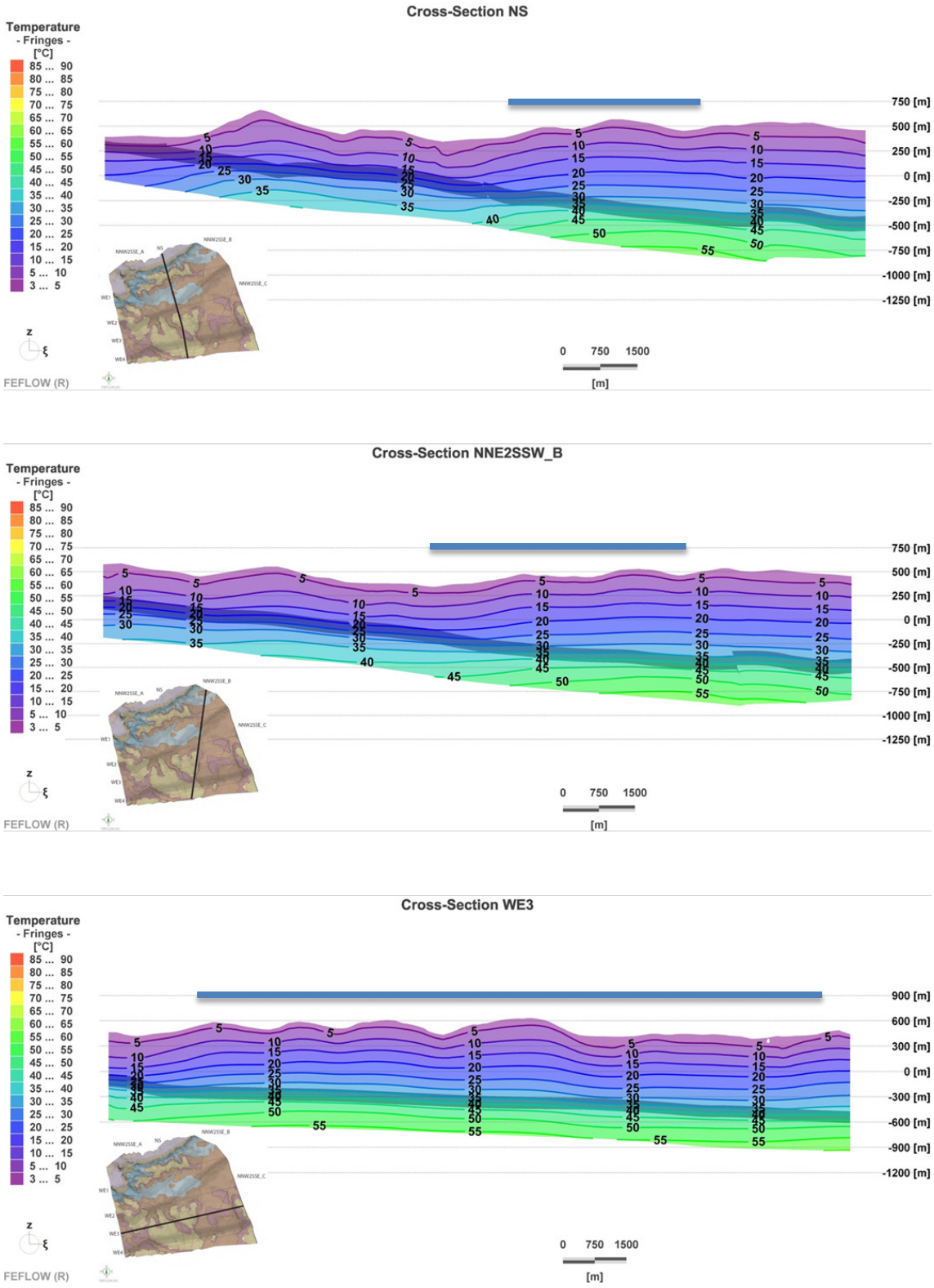

Fig. 3-16: Simulation Variant 2: cross-sectional temperature distribution in the North-South (NS), North/NorthEast-South/SouthWest (NNE2SSW_B) and West-East (WE3) direction. The shaded layer indicates the Opalinus Clay formation. Blue bar indicates the aproximate position of the siting region.

3.4.4 Variant 3

In this simulation, the reference case is modified to take into account spatial variability of basal heat flow assigned to the bottom of the model. Several temperature measurements in boreholes to the west of the model domain resulted in high temperatures indicating a temperature anomaly. In this report it is assumed that these high temperatures are caused by an increased basal heat flow (and not by hot groundwater circulating through faults in which case the heat anomaly would be local and would not affect the siting region). An approximation of heat flow variations is provided through maps of heat flow isolines at the earth surface in Schill et al. (2011). The available data indicates a variation of heat flow in the east-west direction, with values increasing eastwards from Lake Constance towards the Aare and then decreasing again towards Basel. This pattern is approximated for the purposes of the NL local model through a linear gradient applied to the heat flux boundary condition of the model. The average heat flow of 120 mW/m² is therein substituted with heat flow increasing linearly from approximately 105 mW/m² in the east to 135 mW/m² in the west. A qualitative illustration of this approach is shown in Figure 3-17.

Figure 3-18 shows the simulated temperature distributions for the NS, NNW2SSE_B and WE3 cross-sections. Similarly to the temperature distributions obtained when assuming a spatially uniform heat flow (reference case, Figure 3-9), the minimum temperature in the Opalinus Clay is 12 °C at the northern edge of the model (cross-section NS, Figure 3-18). On the other hand, temperature in the deeper parts of the Opalinus Clay reaches approximately 50 °C which is 4 °C lower compared to the corresponding maximum temperatures observed in cross-sections NS and NNE2SSW_B in the reference simulation (Figure 3-9). Similarly, the Opalinus Clay temperatures observed in cross-section WE3 with Variant 3 vary between 27 °C in the west to 50 °C in the east. This indicates that reducing heat inflow in the eastern part of the model reduces temperature in the Opalinus Clay by up to 4 °C, while increasing heat inflow in the western part does not produce a significant change in temperatures in the overlying part of the Opalinus Clay. Weiach is located in the central part of the local model, so that the effect of variable basal heat flow is practically negligible. Temperatures at the top and bottom of the Opalinus Clay in Weiach are 29.8 and 37.8 °C, respectively. The comparison to the reference simulation indicates that the fixed temperature boundary condition at the surface dominates over the fixed inflow boundary at the bottom with decreasing model thickness, such that variations of basal heat flow become more significant for greater formation depths resp. thicknesses of the sedimentary rocks below the ground surface.

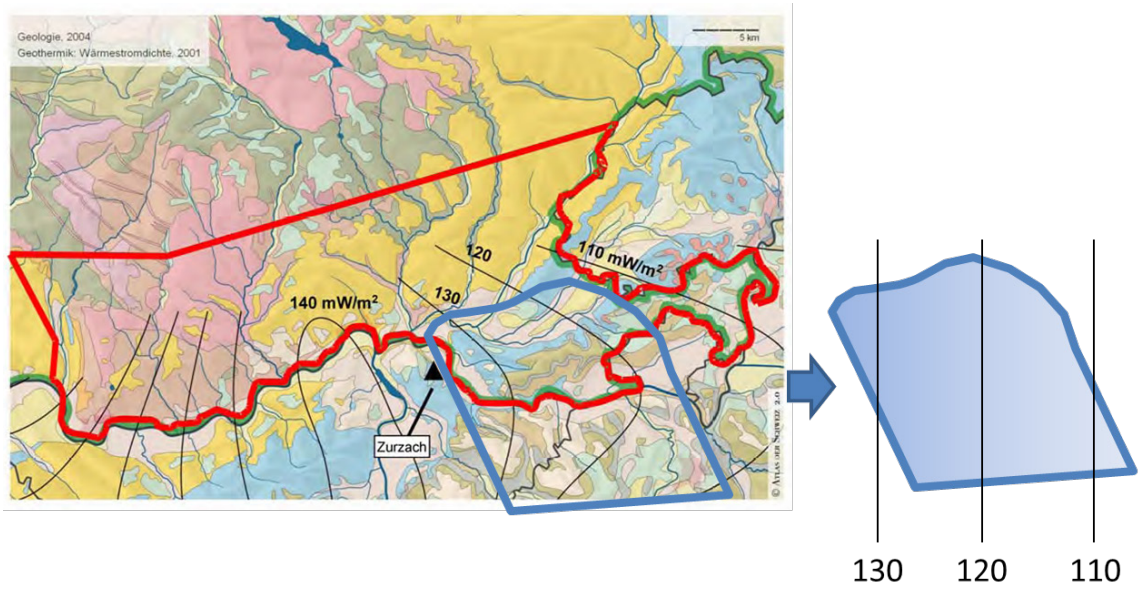

Fig. 3-17: Simulation Variant 3: surface heat flow isolines with the delineated NL local model in Northern Switzerland (left), and the linear heat flow gradient approximation used in Case 3.

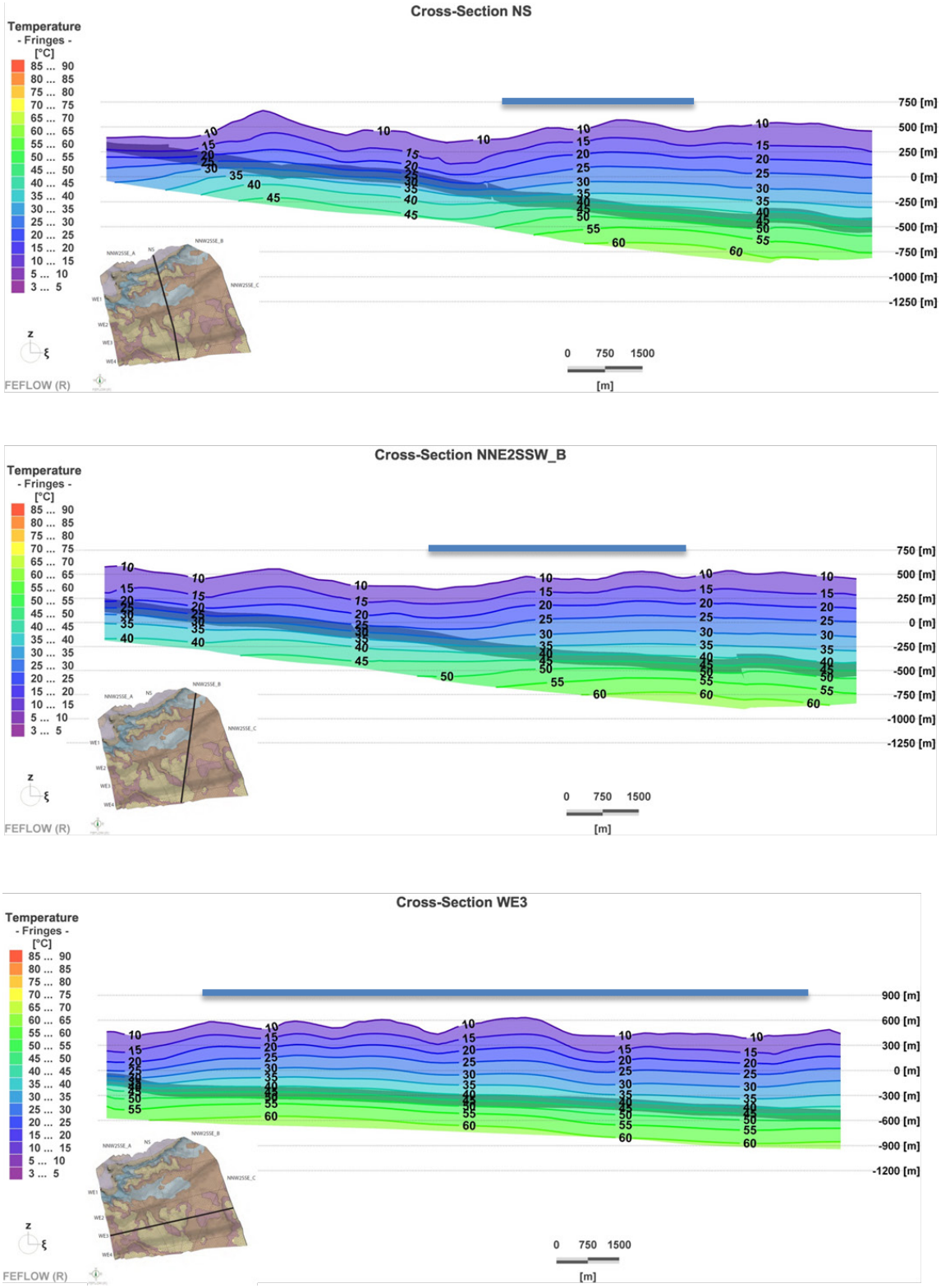

Fig. 3-18: Simulation Variant 3: cross-sectional temperature distribution in the North-South (NS), North/NorthEast-South/SouthWest (NNE2SSW_B) and West-East (WE3) direction. The shaded layer indicates the Opalinus Clay formation. Blue bar indicates the aproximate position of the siting region.

3.4.5 Variant 4

This simulation variant aims at quantifying the impact of natural radiogenic emission of heat from the geological formations on the long-term temperature evolution in the Nördlich Lägern area. In the reference simulation, heat production due to radiogenic activity was neglected. In simulation Variant 4, heat production is assigned to every element of the model domain using the average value of 0.5 μW/m³ as described in Section 2.3. Similarly to the reference simulation, Variant 4 is run until steady-state conditions using a constant temperature of 10 °C at the surface and a fixed heat inflow of 120 mW/m² (or 0.12 J/s) at the bottom.

Figure 3-19 shows a comparison of vertical temperature profiles in Weiach from the reference simulation, simulation Variant 4, and the HRT logs. The plot shows that including the radiogenic heat emission in the model has practically no effect on the temperature distribution. This is due to the fact that the cumulative contribution of rock heat emission across the model domain remains negligible compared to the basal heat flow prescribed at the bottom. This can also be demonstrated with an analytical calculation: if one considers a 1D column constructed with 1x1x1 m³ cells spanning 1000 m from the Muschelkalk base to the surface, the total heat of 5.0e-4 J/s emitted through radiogenic activity is significantly lower than the basal heat inflow of 0.12 J/s at the bottom.

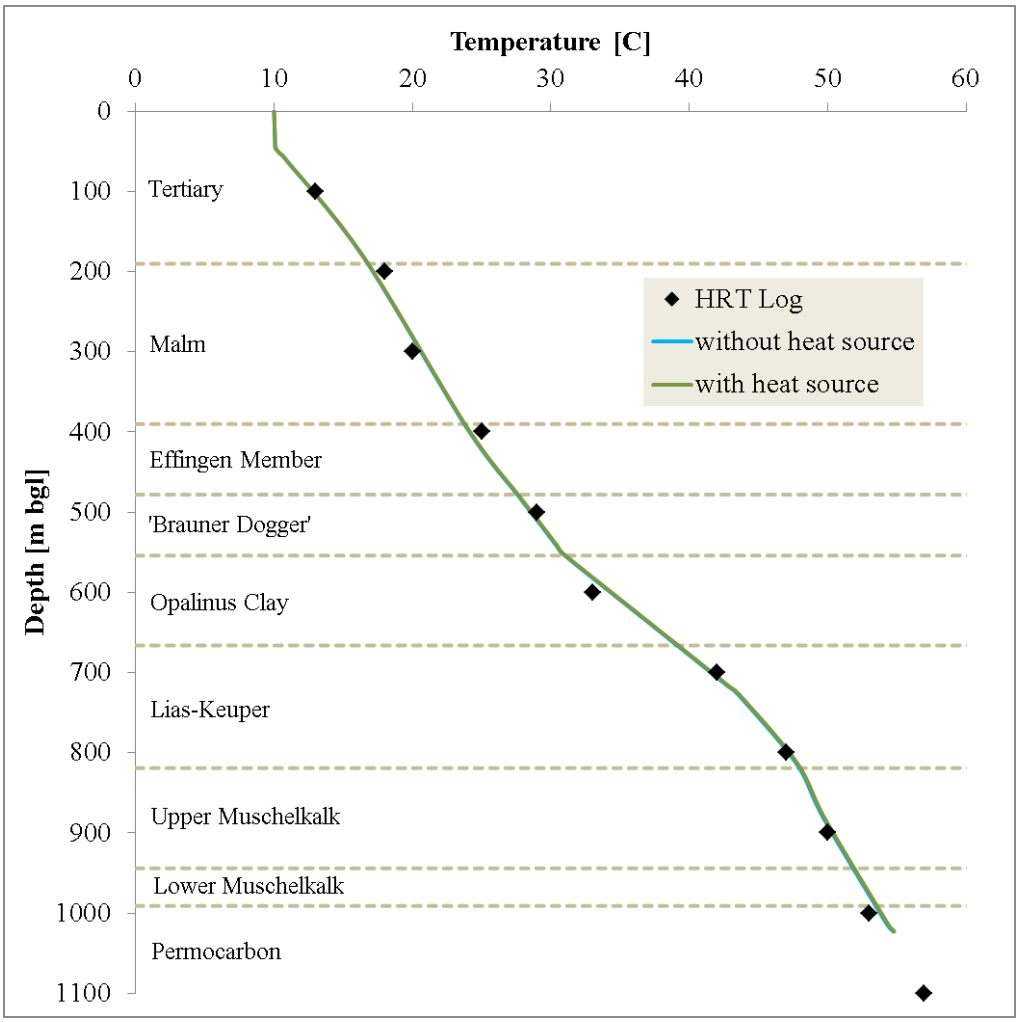

Fig. 3-19: Simulation Variant 4: predicted temperature profiles at the location of the Weiach borehole with and without radiogenic heat generation (reference simulation and Variant 4, respectively).

4 Summary and Conclusions

Modeling the thermo-hydraulic evolution of the siting region Nördlich Lägern is based on the compilation of relevant geothermal data and the subsequent development of a numerical model accounting for thermal effects coupled with groundwater flow. Sources of heat that were taken into account are radiogenic heat emission obtained from logs from the Weiach borehole and basal heat flow determined in Weiach by means of deep borehole temperature measurements and inverse modeling. Additional maps of heat flow compiled for northern Switzerland with several borehole measurements were also considered. Different measurements of temperature were available from the borehole Weiach, with the HRT method providing the most detailed and complete dataset. Specific heat capacity of the rock formations were obtained from lab measurements. Thermal heat conductivities were calibrated using 1D model approximations of the stratigraphic profile from Weiach. These matched calibrated values from previous studies and agree reasonably well with thermal conductivities measured in core samples from Weiach. Additional simulations indicated that the calibrated thermal conductivities can be more suitably used for predicting the temperature profile available from Weiach with the 3D Nördlich Lägern local model. Consequently, the compiled geothermal data and properties have been implemented in a local model originally developed for groundwater flow in order to simulate the coupled thermal-hydraulic behavior in Nördlich Lägern. The developed model was used to carry out simulation variants based on the work scope objectives elaborated in Section 1. While specific minimum and maximum temperatures within the repository site for the different simulations are summarized in Table 4-1, the general conclusions can be summarized as follows:

- Reference simulation: assuming that the average temperature at the surface and basal heat flow through the base of the Mesozoic sediments are constant, this steady-state simulation was used as a basis for comparison to subsequent simulation variants. The reference case indicated temperature isolines forming parallel to the temperature boundary condition at the surface, approximately following the surface topography even at greater depths near the heat flow boundary at the bottom. Larger temperatures were observed accordingly at the parts of the model with larger model thickness (equal to distance between heat source and surface). The maximum temperature in the southeastern part of the model reached approximately 76 °C. Temperatures in the Opalinus Clay varied depending on the formation depth with approximately 30-38 °C at the location of the Weiach borehole. Temperature isolines did indicate some deviation across high-conductive faults spanning through the formations, depressing the simulated temperatures in the deeper section (i.e., mainly below the Opalinus Clay).
- Simulation Variant 1: conductivity of the regional faults spanning through the model domain was set to a very low value so that no advective groundwater flow or convective heat transport through the faults is permitted. The simulation indicates locally higher temperatures compared to the reference simulation that prevail in the southern parts of the model where model thickness is increased.
- Simulation Variant 2: this simulation was performed to demonstrate the transient-state thermo-hydraulic behavior associated with glacial/interglacial temperature variations at the surface. The temperature boundary condition was varied step-wise according to a generic scenario, indicating an impact in subsurface temperatures in the local model through the bottom of the Mesozoic sedimentary formations. Temperatures in the Opalinus Clay in Weiach were predicted to decrease by 6.5 °C at the end of the ice-age period compared to the initial state.

- Simulation Variant 3: based on maps of surface heat flow in northern Switzerland, a spatially variable basal heat flow was assigned at the bottom boundary using the same average heat flow as in the reference simulation. The simulation results indicate changes in predicted temperatures only in the eastern part of the model where temperatures decreased by up to approximately 5 °C. At the location of the Weiach borehole, only a minor decrease of temperatures compared to the reference case is observed with values for the top and bottom Opalinus Clay decreasing to 29.8 and 37.8 °C, respectively.
- Simulation Variant 4: in addition to the properties and boundary conditions used for the reference case, this simulation considered a heat source in the rocks corresponding to radiogenic heat emission. The simulation results did not indicate any significant difference in the predicted temperatures, concluding that radiogenic heat emission can be neglected in similar modeling analyses.

In summary, the simulation results indicate little impact of ambient groundwater flow on the thermal conditions in Nördlich Lägern with the exception of fault zones. The impact of surface temperature variation associated with a potential ice-age indicates a decrease on the host-rock temperature of about 6.5°C. The effect of high-permeability fault zones do indicate a decrease in temperatures mainly in the deeper section of as much as 5°C caused by enhanced heat flow by convection through the high-permeability fault zones. This case was based on a constant heat-flow rate prescribed at the base of the model, corresponding to the bottom of the Muschelkalk. One can expect that locally enhanced heat flow rates along deeper faults and the Permocarbon troughs below the sedimentary formations would result in a potential increase in temperatures mainly in the deeper section below the Opalinus Clay. However, without further knowledge about this assumed heat flow and the location and orientation of such deep faults, simulating such a variant is impossible as the temperature increase below or within the Opalinus Clay would only reflect the postulated increased heat flow within the (unknown) deep fault.

Temperatures for the repository site from the Opalinus Clay are summarized in Table 4-1. Though the reference case and the different simulated variants are based on very different assumptions (e.g. with/without ice age, homogeneous vs. linear increase of basal heat flow etc.), the temperatures in the Opalinus Clay show only little variation. As has been described earlier, temperatures dependent on the depth of the Opalinus Clay within the repository site and range between a maximum of 49.5 °C (deeper parts) and a minimum of 21.5°C (shallower parts).

Tab. 4-1: Site specific temperatures in the Opalinus Clay within the repository site.

	Top OPA		**Bot. OPA**		**OPA min mean [°C]**	**OPA max mean [°C]**
	min [°C]	max [°C]	min [°C]	max [°C]		
Reference	25	45	33	52.5	**29**	**49**
Variant 1	25	45	33	52.5	**29**	**49**
Variant 2	17.5	39	26	46.5	**21.5**	**43**
Variant 3	24	42.5	32.5	50	**28**	**46.5**
Variant 4	25	45.5	33	53	**29**	**49.5**

5 References

Albert W., Blüming P., Heinemann-Glutsch B., Rummel F., Rybach L., Schärli U. & Weber U. (2000): Sondierbohrung Benken, Bestimmung geothermischer Parameter. Unpubl. Nagra Interner Bericht, Nagra, Wettingen.

AXPO (2011): Sensitivity analysis on 1D temperature computations (boreholes Weiach and Benken), Report D1134.1, Axpo AG Neue Energien, Glattbrugg.

Bitterli-Dreher P. (2012): Die Ifenthal-Formation im nördlichen Jura.- Swiss Bulletin für angewandte Geologie 17 / 2, 93-117.

Bläsi H.R., Deplazes G., Schnellmann M. & Trabe, D. (2013): Sedimentologie und Stratigraphie des 'Braunen Doggers' und seiner westlichen Äquivalente. Nagra Arbeitsbericht NAB 12-51. Nagra, Wettingen.

Clauser C., Giese P., Huenges E., Kohl T., Lehmann H., Rybach L., Šafanda J., Wilhelm H., Windloff K., and Zoth G. (1997): The thermal regime of the crystalline continental crust: Implications from the KTB, J. Geophys. Res., 102(B8), 18417–18441, doi:10.1029/96JB03443.

Deslisle G., Caspers G. & Freund H. (2003): Permafrost in north-central Europe during the Weischselian: how deep? ICOP 2003 Permafrost: Proceedings of the Eight International Conference on Permafrost, 21-25 July 2003, Zurich, Switzerland, A.A. Balkema Publishers, Vol.1, 187-191.

Deplazes G., Bläsi H.R., Schnellmann M. & Trabe, D. (2013): Sedimentologie und Stratigraphie der Effinger Schichten. Nagra Arbeitsbericht NAB 13-16. Nagra, Wettingen.

Diersch H.-J. (1998): A shock-capturing finite-element technique for unsaturated-saturated flow and transport problems, in: V.N. Burganos et al (Eds), Computational Methods in Water Resources XII, Vol. 1, Computational Mechanics Publications, Southampton, 207-214.

Finsterle S. (1999): iTOUGH2 User's Guide, Report LBNL-40040, Lawrence Berkeley National Laboratory, Berkeley, California.

Gmünder C., Malaguerra F., Nusch S., Traber D. (2013): Regional hydrogeological model of northern Switzerland. NAB 13-23. Nagra, Wettingen.

Gmünder C., Jordan P., Becker J.K. (2013a): Documentation of the Nagra 3D Geological Model 2012, Nagra NAB 13-28, Nagra, Wettingen.

Haeberli W. (2010): Glaciological conditions in northern Switzerland during recent Ice Ages. Nagra Arbeitsbericht. NAB 10-18. Nagra, Wettingen.

Luo J., Monninkhoff B., Becker J.K. (2014): Hydrogeological model Nördlich Lägern. Nagra Arbeitsbericht. NAB 13-25. Nagra, Wettingen.

Madritsch H., Hammer P. (2012): Characterisation of Cenozoic brittle deformation of potential geological siting regions for radioactive waste repositories in Northern Switzerland based on structural geological analysis of field outcrops. Nagra Arbeitsbericht. NAB 12-41. Nagra, Wettingen.

Nagra (1988): Sondierbohrung Weiach Untersuchungsbericht, Nagra Technischer Bericht NTB 88-08, Nagra, Wettingen.

Nagra (1999): Geologische Entwicklung der Nordschweiz, Neotektonik und Langzeitszenarien Zürcher Weinland, Nagra Technischer Bericht NTB 99-08, Nagra, Wettingen.

Nagra (2000): Sondierbohrung Benken Untersuchungsbericht, Nagra Technischer Bericht NTB 00-01, Nagra, Wettingen.

Nagra (2001): Calculations of the Temperature Evolution of a Repository for Spent Fuel, Vitrified High-Level Waste and Intermediate Level Waste in Opalinus Clay, Nagra Technischer Bericht NTB 01-04, Nagra, Wettingen.

Nagra (2008): Vorschlag geologischer Standortgebiete für das SMA- und das HAA-Lager: Geologische Grundlagen, Nagra Technischer Bericht NTB 08-04, Nagra, Wettingen.

Nagra (2010): Beurteilung der geologischen Unterlagen für die provisorischen Sicherheitsanalysen in SGT Etappe 2: Klärung der Notwendigkeit ergänzender geologischer Untersuchungen, Nagra Technischer Bericht NTB 10-01, Nagra, Wettingen.

Ollinger D. & Baujard C. (2012): Prognose der Untergrundtemperaturen für das Versorgungsgebiet der AXPO AG. Axpo interner Bericht AIB-12-02. Vertraulicher Bericht der Geowatt AG im Auftrag von Axpo, 30.09.2012.

Reisdorf A.G.; Wetzel A.; Schlatter R.; Jordan P. (2011): The Staffelegg Formation: a new stratigraphic scheme for the Early Jurassic of northern Switzerland.- Swiss Journal of Geosciences 104 / 1, 97-146.

Schärli U. & Kohl T. (2002): Archivierung und Kompilation geothermischer Daten der Schweiz und angrenzender Gebiete. Beiträge zur Geologie der Schweiz, Geophysik Nr. 36, SGPK, 140 p.

Schill E., Deckert H., Geiermann J., Koch S., Pohl C., Vierhuis U., Baujard C., Kohl T., Ollinger D., Schütze C., Leven C., Vienken T., Eydam D. & Munoz G. (2011): EGS Technologie Entwicklung: Risikominimierung bei der Exploration, Wissenschaftlich-Technischer Schlussbericht, ITB GmbH.

Appendix A: Sensitivity analyses of calibrations

The 1D column model used for the calibration of thermal conductivities (*iTOUGH2_1D* model) represents the lithostratigraphic profile from the ground surface through the bottom of the Weiach borehole (2'482 m bgl). The calibration was carried out through minimizing least squares of errors compared to temperature measurements spanning depths from 100 m through 2'300 m bgl, wherein the basal heat flow was assigned to the base of the model. Additional analyses were carried out to demonstrate

- the effect of the column length (respective distance of the heat flow boundary condition from the sedimentary formations) on the thermal conductivities estimated for the sedimentary formations assuming steady-state conditions,
- the effect of the column length on the predicted temperature evolution under transient conditions i.e. associated with surface temperature variations during ice ages.

For this, three variants of the *iTOUGH2_1D* model have been implemented as shown in Figure A.1. In the first variant the model extends from the ground surface to a depth of 1'000 m bgl comprising the Mesozoic sedimentary formations and part of the Permocarbon (variant *1D_1000m*). Only the temperature measurements between 0 and 1'000 m bgl are used for the calibration. The second variant extends from the ground surface to a depth of 2'500 m bgl, thus including the Mesozoic sedimentary formations, the entire Permocarbon and about 500 m of the Crystalline (variant *1D_2500m*). In the third variant, the model bottom is extended to 10'000 m bgl assuming that all cells below the base of the Permocarbon have the properties of the Crystalline (variant *1D_10000m*). All three variants assume a constant temperature of 10 °C at the top and a constant basal heat flow of 120 mW/m² at the bottom. The three models are used for calibrating thermal conductivities under the same assumptions. The initial estimates of formation thermal conductivities correspond to the formation average values measured in cores from Weiach (Figure 2-6). The maximum variation around the initial estimates allowed for the calibration is limited to ±0.7 W/m/K. The relative error in the temperature measurements was assumed to be 5%. Comparative calibrations have been carried out for relative errors of 1% and 10% that did not indicate any significant impact on the calibrated thermal conductivities or the goodness of the fit. The formation thermal conductivities calibrated with the three model variants are shown together with the corresponding best fits of temperatures in Figure A-2. It is indicated that in most cases the thermal conductivities are relatively independent from the model length used in the calibration.

The Opalinus Clay thermal conductivity varies between 1.58 and 1.74 W/m/K in the three variants. The thermal conductivities obtained with the *1D_2500m* variant correspond to those of calibration case *iTOUGH2_1D_r1* discussed in Section 3.1 and consequently used for the 3D simulations with FEFLOW. An overview of the best-fit values, standard deviations, and sensitivities are given in Table A.1. The matrix of co-variances and direct correlations obtained with the calibration of the *1D_2500m* model is given in Table A.2. These results yield relatively large variances for the Effingen Member and the 'Brown Dogger', as well as for the Upper and Lower Muschelkalk, which translate into large standard deviations of the estimated thermal conductivities (Tab. A.1). This is due to the limited number of calibration points in these units (Tab. A.1), high correlation coefficients, and the fact that the parameter estimates reached the bounding values (Tab. A.1).

The model depth, determining the distance between the heat flow boundary at the bottom and the temperature boundary at the top of the model, does not affect the steady-state temperature distribution. This was demonstrated here with the 1D model and is also valid for the 3D model

used for modeling the thermo-hydraulic evolution of the NL siting region. However, it may have an impact on the transient-state behavior after a temperature change at the top boundary. In general, decreasing the distance between the top and bottom boundary will lead to a faster equilibration towards the steady-state temperature distribution. Therefore, additional analyses were carried out to estimate the impact of the depth of the heat flow boundary condition on the transient temperatures during an ice age. For this, forward transient simulations of the generic ice age cycle described in Section 3.4.3 were carried out with the *1D_1000m* and the *1D_10000m* model variants. Figure A.3 shows the transient temperature profiles obtained with the two variants at the end of the third phase of the ice age cycle (3 °C temperature at land surface, time -18'000 years). The temperature profile corresponding to steady-state conditions for a land-surface temperature of 3 °C is also shown in the same figure (blue line). It is indicated that the temperatures obtained with the *1D_1000m* variant practically correspond to the steady-state profile. On the other hand, shifting the boundary condition to 10'000 m bgl prolongs the transient state so that temperatures at the end of Phase 3 are higher. The temperature difference between variants *1D_1000m* and *1D_10000m* is 1.4 and 1.9 °C at the top and bottom of the Opalinus Clay, respectively.

The transient behavior in the *1D_1000m* can be viewed as a representation of the 3D model of the NL siting region at Weiach, from the land surface to the base of the Mesozoic sediments. The *1D_10000m* model corresponds to a more realistic representation of heat flow coming from greater depths. It is thus indicated that boundary effects during transient-state conditions introduce a deviation of less than 2 °C for the location of the Weiach borehole, which corresponds to an Opalinus Clay depth from about 550 to 660 m bgl. Greater formation depths corresponding to a deep repository (e.g. 750 m bgl) are found in parts of the model with greater thickness that would accordingly decrease this boundary effect.

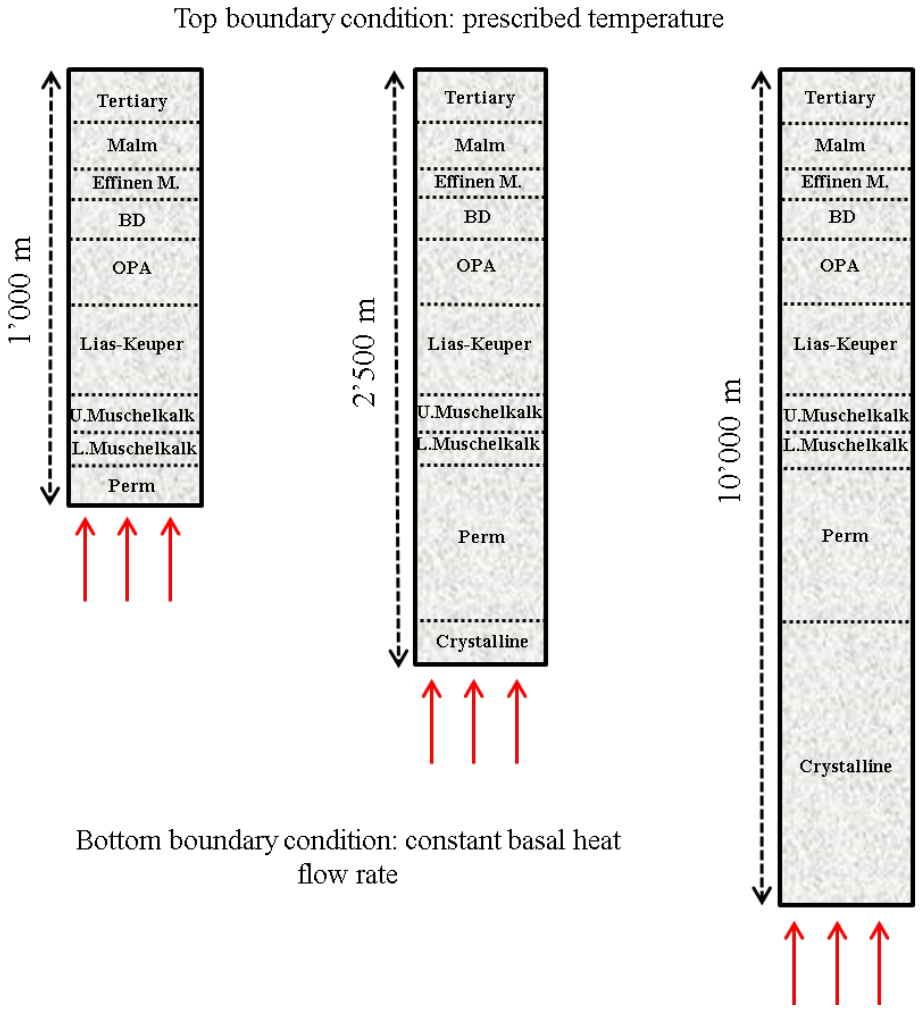

Fig. A-1: Variants of the *iTOUGH2_1D* model assuming bottom boundary at 1'000, 2'500, and 10'000 m bgl.

Formation	1D_2500m	1D_1000m	1D_10000m
	λ [W/m/K]		
Tertiary	3.00	3.00	3.00
Malm	3.70	3.67	3.60
Effingen Member	2.80	2.67	2.57
'Brauner Dogger'	2.80	2.80	2.80
Opalinus Clay	1.74	1.58	1.58
Lias-Keuper	2.50	2.50	2.50
Upper Muschelkalk	4.20	4.50	4.11
Lower Muschelkalk	3.50	3.50	2.92

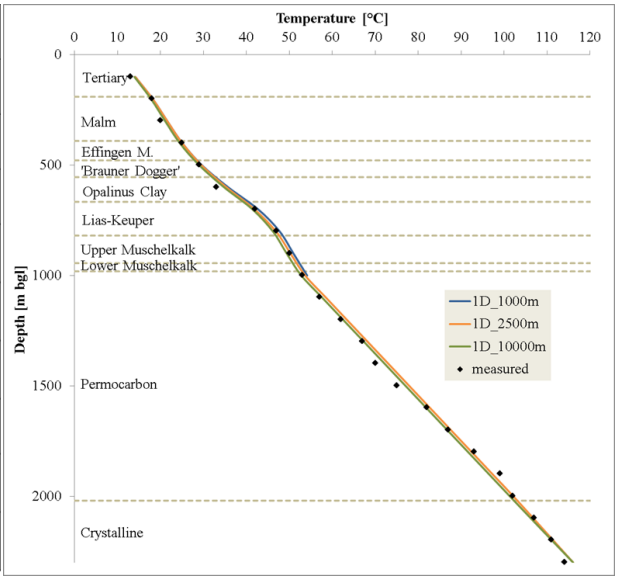

Fig. A-2: Calibrated thermal conductivities and temperature profiles with the three model variants *1D_1000m*, *1D_2500m*, and *1D_10000m*.

Tab. A-1: Best-fit parameters, standard deviations, and sensitivities obtained with the *1D_2500m* model calibration.

	Number of temperature data	Parameter Value		Standard Deviation		Sensitivity	
		Initial	Best Fit	Marginal	Conditional/ Marginal	Output	Obj. Function
Tertiary	1	2.3	3.0 (UB)	0.242	0.553	5.8	0.768
Malm	2	3.0	3.7 (UB)	0.693	0.356	4.2	0.372
Effingen Member	1	2.1	2.8 (UB)	1.767	0.220	1.8	0.143
'Brown Dogger'	1	2.1	2.8 (UB)	3.701	0.135	1.4	0.112
Opalinus Clay	1	2.0	1.74	1.035	0.139	4.7	0.195
Lias-Keuper	2	3.2	2.5 (LB)	1.319	0.184	4.3	0.138
Upper Muschelkalk	1	3.8	4.20	5.539	0.169	1.3	0.068
Lower Muschelkalk	0	2.8	3.5 (UB)	7.903	0.227	0.5	0.029
Permocarbon	11	3.1	2.58	0.153	0.529	10.9	0.323
Crystalline	3	2.7	2.69	0.969	0.821	0.5	0.017

Tab. A-2: Variances (diagonal), covariances (lower triangle), and direct correlation coefficients (upper triangle) of thermal conductivities calibrated with the *1D_2500m* model.

	Tertiary	Malm	Effingen Member	'Brown Dogger'	Opalinus Clay	Lias-Keuper	Upper Muschelkalk	Lower Muschelkalk	Permocarbon	Crystaline
Tertiary	5.9e-2	-0.82	-0.65	-0.60	-0.55	-0.48	-0.43	-0.40	-0.32	-0.12
Malm	-1.1e-1	4.8e-1	-0.87	-0.80	-0.73	-0.64	-0.57	-0.53	-0.42	-0.16
Effingen Member	6.3e-2	-6.0e-1	3.12	-0.95	-0.86	-0.76	-0.68	-0.63	-0.50	-0.18
'Brown Dogger'	-3.8e-2	3.6e-1	-5.1	13.69	-0.96	-0.85	-0.75	-0.70	-0.55	-0.20
Opalinus Clay	6.6e-3	-6.3e-2	8.9e-1	-3.23	1.07	-0.93	-0.83	-0.78	-0.61	-0.23
Lias-Keuper	-4.7e-3	4.5e-2	-6.2e-1	2.26	-1.01	1.74	-0.93	-0.87	-0.68	-0.25
Upper Muschelkalk	7.1e-3	-6.8e-2	9.6e-1	-3.47	1.54	-4.57	30.68	-0.97	-0.76	-0.28
Lower Muschelkalk	-4.7e-3	4.5e-2	-6.3e-1	2.29	-1.02	3.01	-36.2	62.46	-0.79	-0.29
Permocarbon	3.5e-8	4.3e-7	-9.3e-7	7.2e-6	3.5e-6	-3.9e-6	-1.8e-5	-3.6e-1	2.3e-2	-0.53
Crystalline	-3.1e-7	1.1e-6	-1.4e-6	1.5e-5	7.7e-6	-6.6e-6	-3.5e-5	7.1e-1	-7.6e-2	9.4e-1

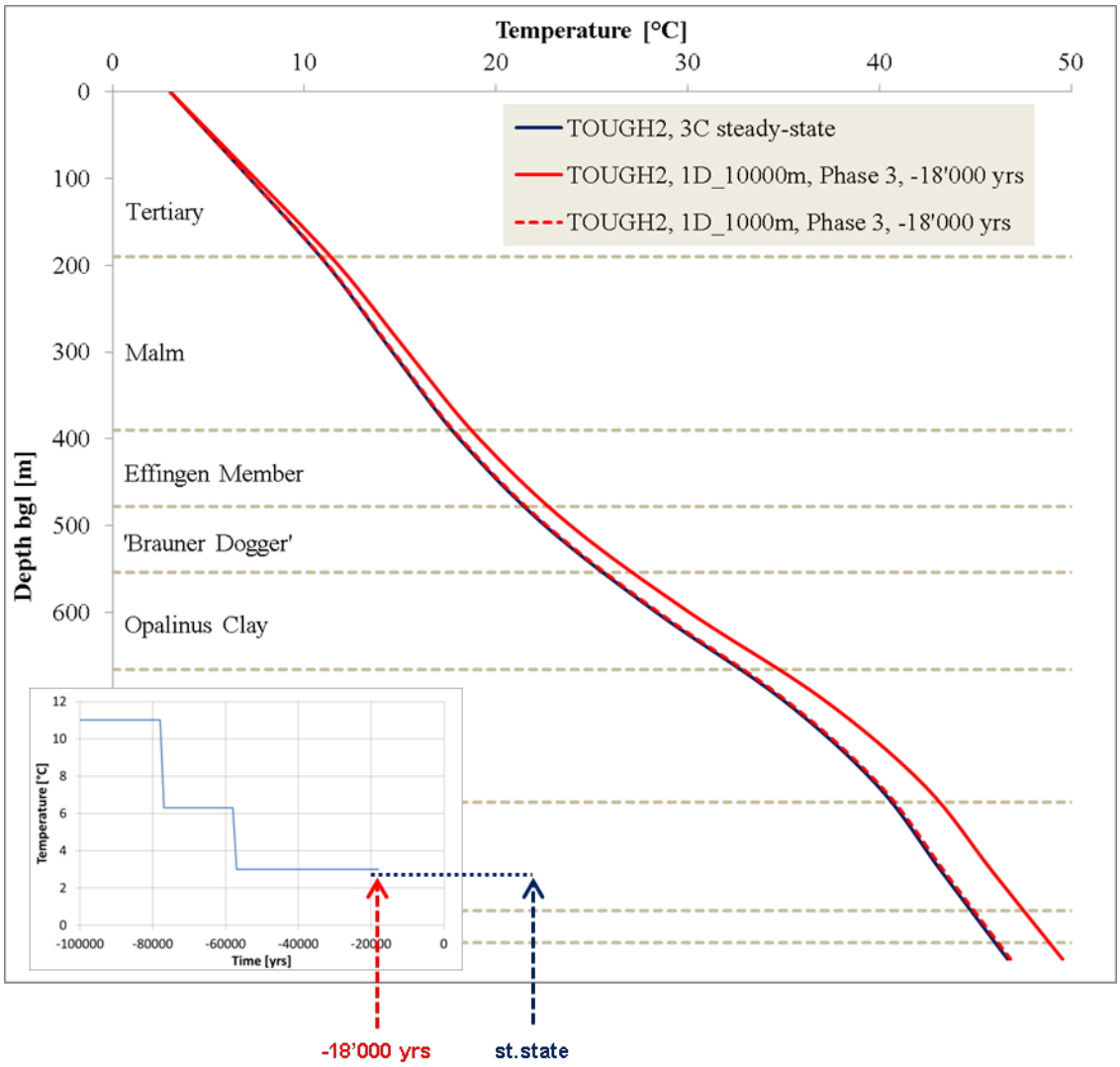

Fig. A-3: Comparison of transient temperature profiles at the end of Phase 3 of the generic ice age cycle obtained with variants *1D_1000m* and *1D_10000m* to the steady-state profile corresponding to a land-surface temperature of 3 °C.